POLITECNICO DI TORINO

Collegio di Ingegneria Meccanica

Corso di Laurea Magistrale
in Mechanical Engineering

Tesi di Laurea Magistrale

A Microfluidic Device for Label-Free Sorting of Circulating Tumor Cells

Relatori

prof. Pietro Asinari
prof. Jie Xu

Candidato

Enrico Grassilli

Luglio 2018

ACKNOWLEDGMENTS

Firstly, I would like to thank prof. Jie Xu that gave me the opportunity to work in his lab on a stimulating and challenging project. He was always attentive to my needs and available to discuss with me problems and solutions.

I am very thankful to Prof. Pietro Asinari for being supportive and available every time I needed suggestions about my work.

I am also thankful to Dr. Guofei Zhou and his post doc Dr. Qiyuan Zhou for providing the cells for the experiments.

I am profoundly thankful to Yang, Jacek and all my colleagues of Microfluidics lab that trained me to use the equipment, helped me whenever I had issues and always made me feel comfortable and supported in the lab.

Then, I am grateful to Tony, Marco, Alfredo, Andrea and all my friends from TOP-TOP-UIC group for helping me and always bringing love and joy to this journey.

Last, but not least, I would like to pay a special thank my family for supporting me financially and always encouraging me during my studies in Turin and Chicago.

EG

TABLE OF CONTENTS

TABLE OF CONTENTS (continued)

CHAPTER **PAGE**

LIST OF TABLES

LIST OF FIGURES

LIST OF FIGURES (continued)

LIST OF ABBREVIATIONS

AC	Alternating current
CTCs	Circulating tumor cells
DC	Direct current
DEP	Dielectrophoresis
DI	Deionized
DLD	Deterministic lateral displacement
DMEM	Dulbecco's Modified Eagle's Medium
EpCAM	Epithelial adhesion molecules
FACS	Fluorescent activated cell sorting
FBS	Fetal Bovine Serum
FDA	Food and Drug Administration
LOC	Lab on a chip
NCF	Nanotechnology Core Facility
nDEP	Negative DEP
PBS	Phosphate buffered saline
pDEP	Positive DEP
PDMS	Polydimethylsiloxane

LIST OF ABBREVIATIONS (continued)

RBC	Red blood cell
SDS	Sodium dodecyl sulfate
WBC	White blood cell

SOMMARIO

Questa tesi presenta un nuovo metodo per la separazione di cellule tumorali circolanti o CTC in campioni di sangue, dimostrando sperimentalmente il concetto alla base di questa tecnologia.

Il cancro é una delle principali cause di morte nel mondo. L'umanitá compie continuamente sforzi enormi per ridurre le morti dovute al cancro e negli ultimi decenni i miglioramenti sono stati notevoli. Il tumore metastatico rimane tuttavia pressoché incurabile per la maggior parte dei pazienti. La metastasi é uno stadio avanzato della malattia che consiste nella diffusione tramite l'apparato circolatorio di cellule tumorali provenienti dalla massa originaria. In questo caso la prevenzione e il trattamento tempestivo sono cruciali per evitare che il tumore in avvio di metastasi si espanda. Ogni anno si sviluppano nuove tecniche di diagnosi non solo per individuare, ma anche collezionare cellule tumorali in circolo. Queste cellule sono poi analizzate per fornire ai pazienti trattamenti mirati e di maggiore efficacia.

La Microfluidica ha un ruolo centrale nello sviluppo di queste nuove tecniche, che sono presentate nell'introduzione di questa tesi. Il dispositivo qui presentato combina due comuni e promettenti tecniche, il DLD o deterministic lateral displacement , che viene utilizzato per separare cellule di dimensioni diverse e la dielettroforesi o DEP , per intrappolare selettivamente i globuli bianchi. Nel capitolo 2 vengono spiegati la teoria e i metodi di fabbricazione del dispositivo. Nel capitolo riguardante gli esperimenti sono stati sottoposti alla prova quattro diversi design di DLD, utilizzando microsfere di polistirene e cellule tumorali A549, modificando i buffer e applicando campi elettrici in corrente alternata con diversi valori di tensione e

frequenza. L'obiettivo finale era di ottenere da questi esperimenti la separazione delle CTC in campioni di sangue. La scelta di eseguire gli esperimenti con microsfere di polistirene é stata dettata dalla necessitá di semplificare le procedure e ridurre i costi di una soluzione ancora allo stadio embrionale. Ciononostante, i risultati non solo confermano questo concept, ma, addirittura, incoraggiano a proseguire con ulteriori esperimenti, utilizzando prima globuli bianchi e poi campioni di sangue completo. La viabilitá dell'80%, mostrata dai test di viabilitá a 650-750 volt, é pure promettente. Per migliorare le performance quali throughput, portata ed efficienza della separazione la larghezza del canale principale puó essere aumentata oppure si possono utilizzare piú dispositivi in parallelo, con conseguente aumento dei portali di ingresso e uscita. Riguardo la comparazione dei diversi design con simile diametro critico si é notato come, a paritá di portata, i canali aventi i pilastri piú vicini tra loro intrappolino meglio le particelle. Inoltre, pilastri piú grandi possono trattenere piú particelle, aumentando l'efficienza dell'array.

CHAPTER 1

INTRODUCTION

Microfluidics has experienced a huge development over the last few decades, nowadays it finds application in many different fields as bioengineering, medicine, medical sciences, drug delivery, electronics, reagent/liquid sample analysis, healthcare and defense [4]. Lab on a chip (LOC) is an interesting and useful concept of diagnostic using microfluidics. It transfers to microscale common lab testing techniques like sample analysis with chemical reagents. Some examples are transporting samples between different micro-chambers and separation methods to provide purified biological material for further analysis. Microfluidics devices are also used for sorting different particles in a sample based on their size. This technology has application in food processing industry, biological and chemical research [5][6]. In biological application, the separation of damaged, dead and infectious cells from the healthy ones is fundamental in disease diagnosis, prevention and monitoring [7]. In particular, cells are manipulated on the base of different chemical and physical properties such as size, stiffness, electric/magnetic conductivities, etc [8]. "In 2017, 1,688,780 new cancer cases and 600,920 cancer deaths are projected to occur in the United States. "[9] The 90% of these deaths from cancer are related to the so-called malignant tumors. [10] In a Malignant tumor cells migrate (metastasis) to other areas of the body as the disease progresses. The prognosis for patients with this tumor is by far worst then the one for localized cancer as their survival rate drops significantly. For example, after the spread of a localized breast cancer into different organs the patient survival

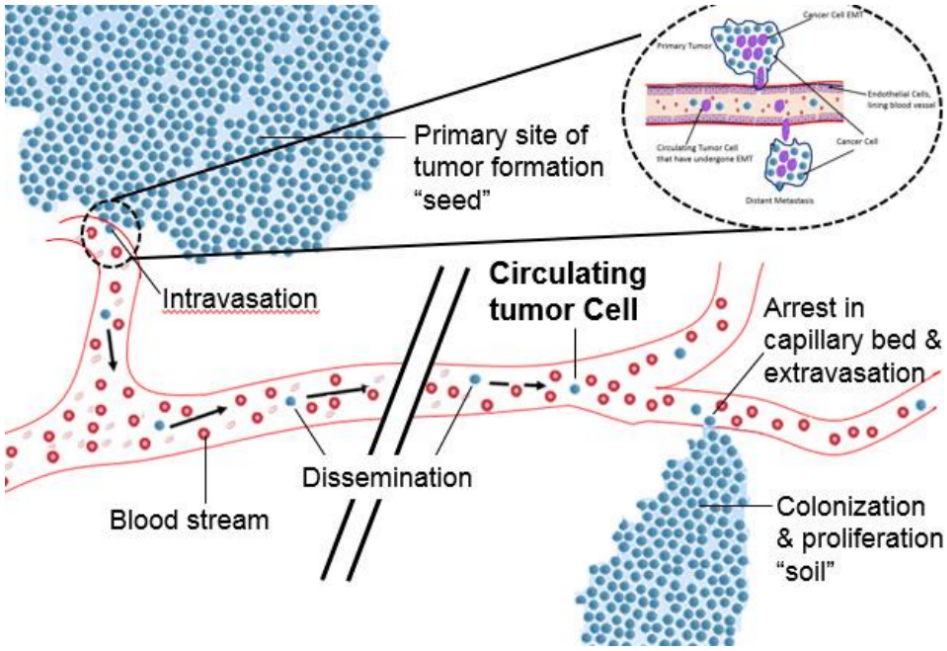

Figure 1: Metastatic Tumor spreading mechanism.

rate falls from 98.6 to 23.4%.[11] As a tumor mass expands and requires more nutrients a new vascular system grows around the initial site. This phenomenon is called tumor angiogenesis, these new blood vessels provide a route for detached tumor cells to enter the blood stream and origin metastasis. From this point the cells can easily reach lymph nodes and distant organs, spreading the disease all around the organism. [12] In this early cancer seeding the number of circulating tumor cells (CTCs) is as low as 1 cell/ml.[13][14] For this reason, the monitoring instruments must be very sensitive to ensure early detection and treatment. Unfortunately, diagnostic techniques used nowadays, as imaging studies or serum marker assays, have high rates of false negatives.[15]

Cells detection and batch processing for further analysis is another promising diagnostic tool as CTCs can be used as a liquid biopsy to study the original cancer properties and test the response of new drugs. [16][17] FDA-approved CellSearch TM (Verdex, USA) can detect CTCs by binding ferrofluid nanoparticles to epithelial adhesion molecules (EpCAM) using the anti-EpCAM antibody. Then, thanks to a magnet it captures the cells from blood samples. Even if this method is highly sensitive, it lacks the capability of identifying the original tumor or distinguish between different CTCs that may be present in the patient, since EpCAM and other biomarkers utilized are general to many tumors.[18] Moreover, cell sample handling and chemical treatment brings to a sensitive cell loss, reducing the number of cells available for analysis. These problems brought researcher in the field of cell separation to look for solutions that can deal with the different chemical and physical properties of cells. Microfluidics Lab on a Chips (LOC) resulted to be an interesting options for cell sorting and over the last years many articles reported the use of microfluidics devices to isolate CTCs.[19] Before going into detail with the solution proposed in this thesis, an outlook over microfluidic separation is here presented.

1.1 Microfluidics separation: Categories

Microfluidic devices represent a step further toward the perfect platform for cell sorting. The compact design, precise control and flexibility make them a miniaturized version of an entire lab. These fluidic systems manipulate small cell samples and chemicals with the possibility to integrate in the same LOC bio-mimicking, bio-sensing, physical and chemical testing together with useful operations as counting, mixing, lysing and focusing. The volume of samples is in the

order of microliters and to be considered micro the device dimensions must be smaller than 100 micrometers. The possibility to use standard microfabrication procedures for the manufacturing of these devices has made them cheap and easy to build, widening the market. Together with low cost there are many other advantages presented by this technology. First, the performances as throughput, resolution and sensitivity are higher than the average, and furtherly enhanced by the ability to combine more different systems together. Moreover, cell loss is drastically reduced by the continuity of the device that eliminates the need for transportation of samples from one step to another (loading, isolation and recognition are all made in the same platform). Microfluidic separation devices rely on different recognition mechanism, according to this we can distinguish three main categories [2]:

(i) fluorescent label-based;

(ii) bead-based;

(iii) label-free sorting.

1.1.1 Bead-based cell sorting

This system relies on the capacity of some particles to target or non-target cells depending on characteristics as material, surface-binding and size. The bounded cells will now respond due to an external field applied in a different way than the unbounded ones. One of the main advantages of this method is the faster rates at which samples can be sorted thanks to the possibility of targeting the cells in clusters and not only singularly. Miltenyi et al. proposed

in 1989 the first ever commercial system implementing bead-based cell sorting. Soon the cell isolation system was scaled down for microfluidics applications.[20]

1.1.2 Fluorescent Label-based cell sorting

Fluorescent label-based cell sorting identifies different cells in a sample using fluorescent probes and cell staining. Traditional FACS (fluorescent activated cell sorting) arrange cells in a laminar stream that is scanned by a laser beam, when the focused light hit the cell it scatters into a detector. Then the signal is analyzed to determine the cell type and sort them. In FACS, instead, an aerosol droplet encapsulates a single cell, then it is electrostatically charged and sorted.[21] This method is really efficient, being cells treated one by one. Furthermore, the process of staining is faster and more reliable than labeling by bead-based methods, granting a better precision during experiments. These characteristics made fluorescent label-based sorting more convenient with respect to bead-based labeling and so a preferred solution in cell sorting microchips.

1.1.3 Label-free cell sorting

Label-free sorting is the most interesting of the here presented categories because it includes not only the so-called active systems such as cells labelling using surface markers but also passive ones. Passive systems rely on physical properties of cells to perform more variegated sorting, for example by shape, size, density, elasticity, magnetic susceptibility and polarizability. Another great value of label-free sorting is the short amount of time needed to prepare the device, in cells sorting this is crucial, increasing the viability of the sample and making this technology even more attractive.

1.2 Microfluidic separation: Governing principles

For every category a subsequent differentiation can be made according to physical, chemical or electrical principals adopted for cells sorting. Some of these can be applied to all of the previously cited categories, while others are adaptable only to a specific one. For example, passive systems can be exploited only for label-free sorting while magnetophoresis is a prerogative of marker-based systems. The state-of-the-art of sorting methods is here partially presented, citing some devices for every different category.

1.2.1 Electro-kinetics

Electro-kinetics refers to the effects of the application of an electric field on particles and cells, that due to electrostatics phenomena experience a displacement from the initial position.[22][23] Beside sorting cells into charged aerosol as in FACS, electro-kinetics are used to move cells into the flow stream. It can be distinguished three main types: electrophoresis, di-electrophoresis and electroosmotic flow. All these phenomena involve forces that are suitable for sorting at microscale. These methods can be used for non-sequential sorting, being the forces involved dependent on size and intrinsic electrical properties of particles.[22] The strength of electro-kinetics sorting is the possibility to apply it in all the previously cited categories. We have examples in bead-based sorting where the adhesion of beads to target cells results in a stronger DEP force experienced from the compound.[24] Méance et al. used an electro-hydrodynamic principal to perform label-free sorting of DNS particles in viscoelastic fluids.[25]

1.2.1.1 Electrophoresis

It is the displacement of charged cells or particles in the direction of the oppositely charged electrode due to a uniform electric field generated via direct current (DC). In most of the cases the cell membrane presents chemical groups that induce a negative charge to the cells. So, the force exploited by the DC field to the particle will be toward the positive electrode and proportional to its charge density.[22] Takahashi et al. performed downstream sorting by electrophoresis, labelling with a fluorescent marker the cells and analyzing them under the focused beam of an upstream laser detector.[26] Recently, Guo et al. presented a device capable of high throughputs by electrophoretic sorting a continuous flow of water-in-oil droplets.[27] The cells were pre-focused and then singularly encapsulated in droplets.

1.2.1.2 Dielectrophoresis

When a nonuniform electric field is applied cells and particles experience a force, due to an induced polarization of the particle itself. This di-electrophoretic force is experienced by both charged and uncharged particles, due to the difference of permittivity and conductivity between particles and the buffer in which those are immersed. Depending of the gradient of an alternating current (AC) field the particles will either move toward regions where the field is stronger experiencing pDEP (positive di-electrophoresis) or where it is weaker by nDEP (negative di-electrophoresis). The pDEP occurs when the electric permeability of the particle or cell is higher than the one of the buffer, while in the opposite case entities experience nDEP.[22] In cell sorting nDEP is preferred because effects on cells viability are less severe than in pDEP. In label-based sorting Mazutis et al. exploiting DEP in downstream sorting

demonstrated that encapsulation of cells and capture of antibodies-coated beads together into emulsions makes possible to analyze cells secretion of antibodies (Figure 2). [1] Label-free sorting widely uses DEP for separation of cells and particles based on dielectric properties as conductivity, polarizability or permittivity. The first to apply this concept was Huang et al., using a microelectronic array to sort five different cell lines.[28] Cummings et al. exploited the nonuniformities obtained by applying an electric field over an array of insulating posts to exert different forces to cells passing through the device. [29]

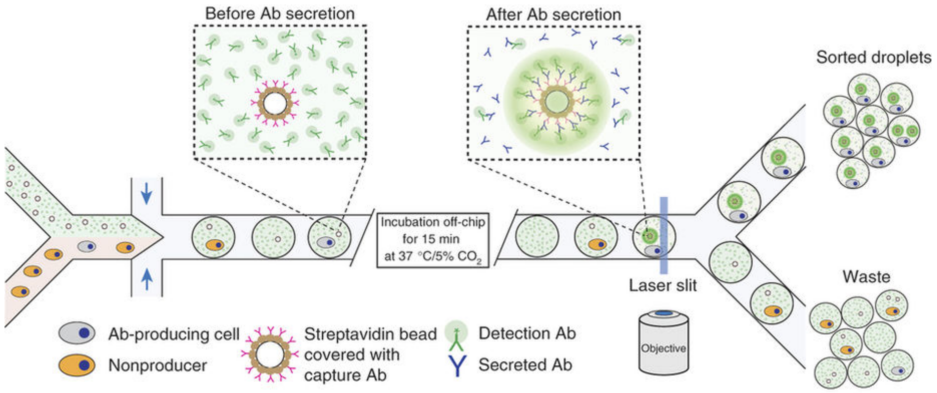

Figure 2: Droplet-based microreactor for cell sorting using DEP. Reproduced with permission from [1]. Copyright 2013 Nature Publishing Group.

1.2.1.3 Electroosmotic flow

Electroosmotic flow instead of moving particles or cells, like in DEP and electrophoresis, moves the surrounding fluid thanks to ions in the solution and together with the fluid moves

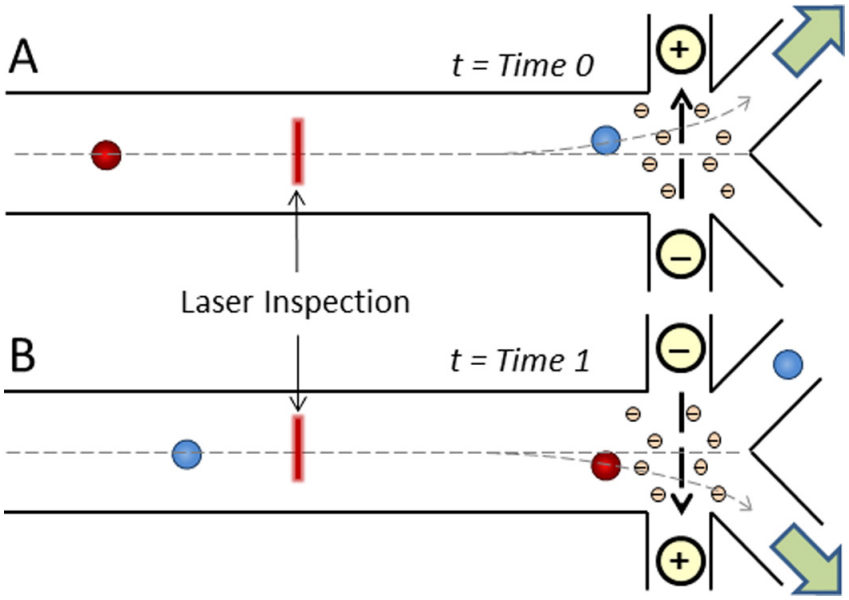

Figure 3: Electroosmotic device for cell sorting exploiting DC current. Reprinted with permission from [2]. Copyright 2015 Royal Society of Chemistry.

everything that is carried by it (Figure 3) [30]. A serious drawback of this method is the generation of bubbles and chemical at the elecrodes due to the electrolysis of electrolyte. These phenomena can complicate device operations and damage cells, affecting the viability. [31]

1.2.2 Passive cell sorting

These systems rely on morphologic characteristics of cells and biological particles and operate the separation based on their different shape, size, density or stiffness. No labelling is used in passive systems. The most common methods include deterministic lateral displacement, inertial focusing, hydrodynamic spreading, transient cellular adhesion, filtration and cellular immobilization.[32]

1.2.2.1 Deterministic Lateral Displacement

A deterministic lateral displacement (DLD) system is made of a micropattern of various figures into the microchannel where the sample flows. The array is arranged to create a different possible route for the cells, depending on their size. When flowing through this complex channel the fluid tends to arrange its motion in streamlines that follow the gradient of pressure imposed by an external force. If the cells transported by the buffers have a diameter that is smaller than the critical one defined by the geometry of the array, then they remain into the streamlines, following the flow direction. Instead, if the diameter is bigger, cells will exit the streamline and bounce over the obstacles of the array, following the direction imposed by its geometry (Figure 4)[33]. These micropatterns can be easily produced with standard microfluidic chips fabrication methods. This system has been used to sort cancer cells from undiluted blood samples [34]. As mentioned, deterministic lateral displacement can be used for cells sorting based on shape and deformability as showed by Beech et al. [33].

1.3 Device concept

After analyzing the state-of-the-art of microfluidics an original idea to improve performances of this technology is here presented. In this work a focus is made on circulating tumor cells (CTCs) isolation from blood samples and analysis, so the most important requirement is to obtain high viability and provide label-free cancer cells to be used in further analysis. First, the device must be easy to produce using standard microchips fabrication procedures to maintain the costs low and the materials biocompatible. The traditional procedure of soft lithography with polydimethylsiloxane (PDMS) has been used, that fitted perfectly our requirements of bio

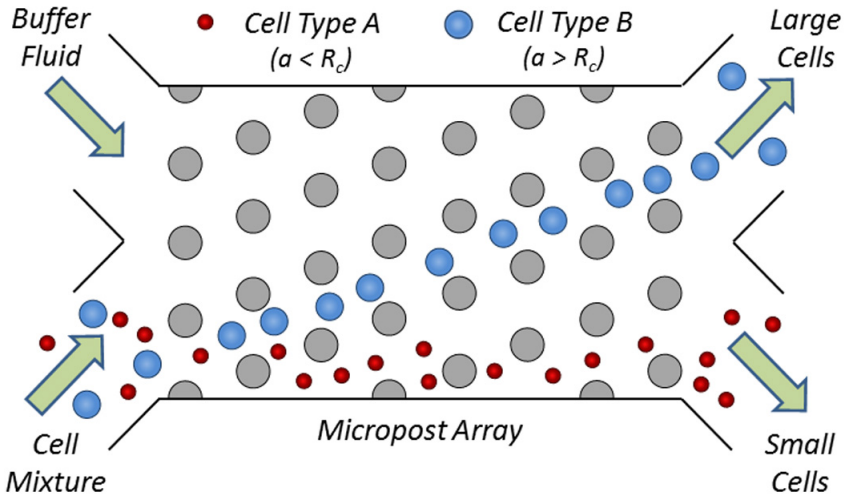

Figure 4: Deterministic Lateral Displacement device scheme. Reprinted with permission of [2]. Copyright 2015 Royal Society of Chemistry.

compatibility and electric insulation. Then, the device must be able to isolate tumor cells from the hemocytes, this means that a size-based sorting would not be sufficient, since white blood cells (WBCs) have the same size as our target cells. From here the need to integrate a size-based method with another one that relies on other properties. To maintain a high viability the time needed for sorting must be kept short, then a sufficiently high flow rate is required. Finally, good throughput is fundamental in this case, since the number of CTCs contained in blood is tremendously low in early-stage metastatic cancer. The proposed device addressed all the cited points by combining a deterministic lateral displacement (DLD) array and an electric field to exploit di-electrophoresis and trap target cells. In this way, particles can be sorted by size and dielectric properties in the same device. Together with circulating tumor cells the sample will include red blood cells (RBCs) or erythrocytes, white blood cells (WBCs) or leukocytes and

platelets. RBCs are smaller than WBCs and CTCs so to sort them it is sufficient to set the DLD critical diameter to a value in between RBCs diameter, that is approximately of $5\mu m$, and WBCs and CTCs diameter, around $10\mu m$. Then the isolation of CTCs will be achieved by trapping WBCs in the DLD array, exploiting the negative DEP force generated by an alternate current (AC) electric field. (Figure 5) The field is obtained by introducing two electrodes in dedicated reservoirs connected to the main channel. With this configuration the AC electric field is "horizontal", meaning that it has the same direction as the flow rate. CTCs will be collected at the top outlet of the DLD channel, WBCs remain trapped in the array, and red blood cells are discarded at the bottom outlet of the device.

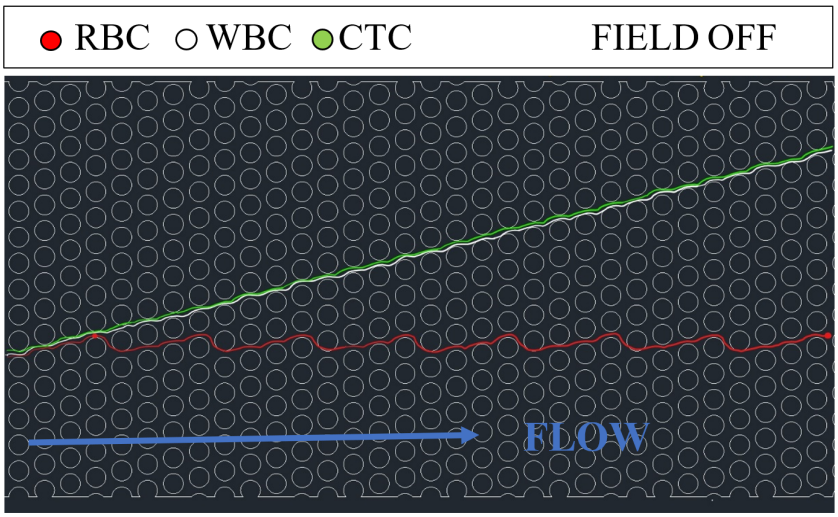

(a) Device concept field off.

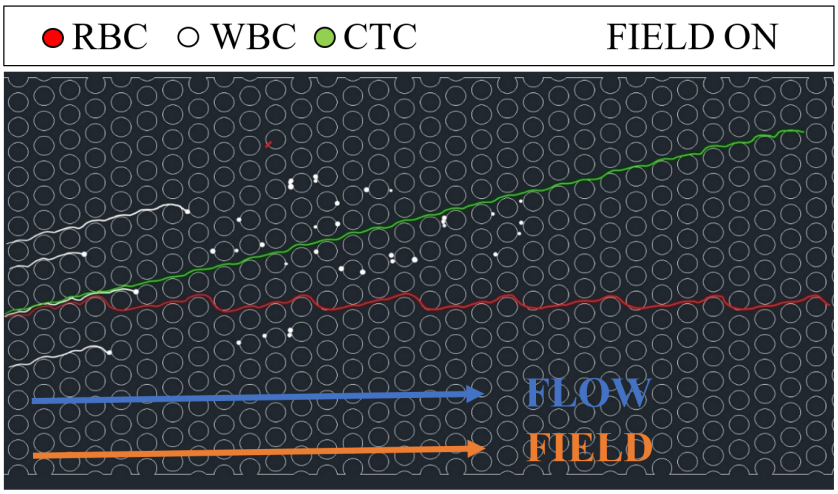

(b) Device concept field on, WBC get trapped.

Figure 5: Device trapping concept, part 1. RBCs are separated from WBCs and CTCs having a size smaller then the critical diameter of the DLD array.

A similar configuration was previously used by Beech et al. to show the potentialities of tuning the DLD array by nDEP. [3] Anyway this device was exploiting the nDEP force to tune the critical diameter of DLD by forcing particles with smaller diameter to displacement mode and not trapping them. Moreover, even if this technology has been used for characterization of biological particles and cells [35], it represents a completely new approach in CTCs isolation in microfluidics.

CHAPTER 2

THEORY AND METHODS

To better understand the potential of this method a detailed explanation of its working principals is presented in this chapter. First, DLD theory and design guidelines are shown, being deterministic lateral displacement the base of this concept. Then DEP theory is presented, explaining more in detail the dielectric parameters on which this force depends and focusing on insulator based di-electrophoresis (iDEP), a powerful technique widely used for cells and particle trapping [36]. Then, the complex electric field generated by the insulator array of different possible geometries is compared. To model the electric field a simple simulation with COMSOL multiphysics has been prepared and run. Once the main players have been discussed, a qualitative analytical balance of forces is made, to evaluate for which theoretical conditions it is possible to obtain particle and cells trapping. The last two paragraphs explain the choice of final designs and the procedures used for the fabrication of devices.

2.1 DLD Theory

Deterministic lateral displacement is a passive sorting method that, thanks to an array of posts into a microchannel, is able so separate particles and cells of different size. Rows of pillars are tilted at a fixed angle, maintaining the same distance between each row and each post in the same row. These two parameters, gap and angle determine the critical diameter for which particles will be sorted. The streamlines into the channel are created by this shift of pillars

rows at the designed angle. The first streamline width and particles size are the responsible for the DLD sorting. With first streamline it is meant the one closer to posts, where the flow is slower due to shear stresses between fluid and pillars.If the particle is big enough to have its hydrodynamic center out of the limit of the first streamline it will move to the adjacent lamina, bouncing on the following pillar. If, instead, the center of the particle is within the width of the streamline, it will move through all the array remaining in the same lamina and dodging the pillars drawing a characteristic zig-zag movement (Figure 18).

DLD systems has been developed for microfluidics chips and at this microscale they must deal with phenomena that at macroscale are usually considered secondary or negligible. Laminar flow, diffusion and fluidic resistance become crucial in the physics of this devices, while effects from inertial flow are less important [37]. For this reason, the fluid mechanics of DLD is presented in the next section, building the basis to understand the working principles of this technology and finally explain its design criteria.

2.1.1 Microfluidics fluid mechanics

At this scale the fluid is typically laminar and easily predictable since viscous forces dominate inertial forces. The Navier-Stokes equation for incompressible fluid is:

$$\rho\left(\frac{\partial v}{\partial t} + v \cdot \nabla v\right) = -\nabla p + \eta \nabla^2 v \tag{2.1}$$

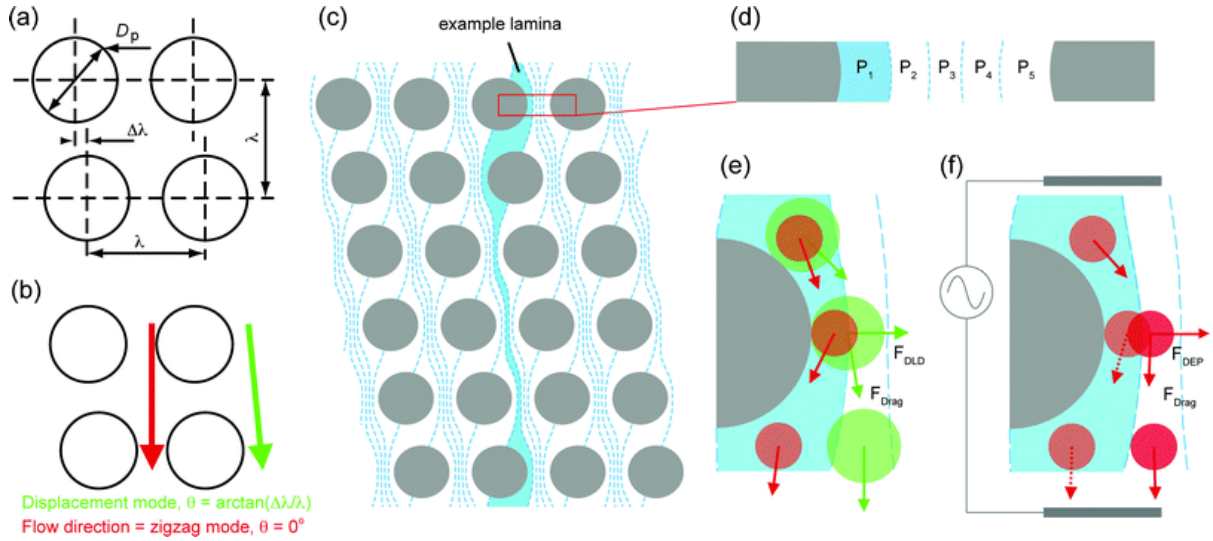

Figure 6: DLD principle. Reprinted with the permission of [3].

Where ρ is density, v is velocity, p is pressure and η is viscosity of the fluid. Being inertial effects negligible, the non-linear term $v \cdot \nabla v$ can be neglected. So, the Stokes equation is obtained:

$$\rho \frac{\partial v}{\partial t} = -\nabla p + \eta \nabla^2 v \tag{2.2}$$

From the Stokes equation, the Reynolds number Re is derived. It shows the ratio of inertial to viscous force densities:

$$Re = \frac{\rho v D_H}{\eta} \tag{2.3}$$

Where D_H represents the hydraulic diameter. It is calculated as:

$$D_H = \frac{2wh}{w+h} \tag{2.4}$$

w and h are respectively width and depth of the microchannel. A Reynolds number below 2000 indicates that the considered fluid is in laminar flow, above 2000 the flow becomes turbulent. In microfluidics this number is usually below 1 [37]. This means that, except for diffusions effects, two different fluids do not mix. This makes flow prediction easy and the designing process more reliable and consistent, facilitating the control of moving particles.

As stated before, diffusion is the only phenomenon that causes mixing in microchannels. Usually, for particles of micrometer size the diffusion effect is negligible for a DLD, but when particle size decreases it can affect their trajectories over the array [37]. The dimensionless number used to compare the effects of convection over diffusion of particles in motion in a fluid is the Peclet number Pe:

$$Pe = \frac{vw}{D} = \frac{diffusion\ time}{convection\ time} \tag{2.5}$$

Where D is the diffusion coefficient calculated by the Stokes-Einstein equation for spherical particles:

$$D = \frac{kT}{6\pi\eta a} \tag{2.6}$$

In this equation k is the Boltzmann constant, T the temperature in kelvin, and a the hydrodynamic radius of the particle. In microchannels this number ranges usually between 10 and 105, indicating that convection is predominant in these devices [37]. Considering an example for our case, assuming a maximum velocity of $2000\mu m/s$, a diffusivity of $0.02\mu m^2/s$ for a white blood cell with a diameter of $10\mu m$ in a channel wide $20\mu m$ then according to Equation 2.5, the Peclet number will be 2,000,000. Then, considering a channel height of $40\mu m$ and water as buffer (density $1kg/ml$ and viscosity $1mPa \cdot s$) the Reynolds number results to be 0.053, definitely smaller than 1, confirming the prevalence of viscous effects over inertial ones.

An important parameter for the design our device is fluid resistance. When passing through a channel a fluid experiences a resistance that increases as the dimensions of the channel decrease or the geometry gets more complex. As a result, a difference of pressure is generated between the inlet and outlets of the device, following the relation:

$$Q = \frac{\Delta p}{R} \tag{2.7}$$

Where Q is the flow rate, R a resistance coefficient and Δp the difference of pressure driving the flow. When considering high aspect ratio rectangular microchannels of length, the resistance is calculated as:

$$R = \frac{12\eta l}{wh^3} \tag{2.8}$$

Usually, height is predominant over channel width in DLD devices; in this case the parabolic flow profile is determined by the gap between posts and Equation 2.8 becomes:

$$R = \frac{12\eta l}{hw^3} \tag{2.9}$$

Davis derived an empirical formulation for resistance through the array of a DLD geometry by running finite element method (FEM) simulations on COMSOL for different values of posts gap and channel height [38]:

$$R \simeq 4.6 \cdot \left(\frac{\eta\beta}{\alpha G^2 E}\right) \tag{2.10}$$

Where α is the width of the array section, β is the length of the array section, G is the gap between posts and E the height of the channel. The formulation was developed considering post diameter equal to the gap between posts and ϵ of 0.1 (ϵ is the shift coefficient). A quick estimation of the resistance in the array is provided using Equation 2.10 and assuming the length of the array equal to $8mm$, $R = 7.5e9Pa \cdot s/m^3$.

The shear stress that a biological particle experiences in a channel may affect its characteristic or damage it. For this reason, an estimation of the shear stress in our channel can prevent

damaging blood cells running through the device. We can evaluate the shear stress acting on the particles flowing through the pillars with a simple model that starts from newton definition:

$$\tau = \eta\gamma \tag{2.11}$$

The shear stress τ is linearly dependent by the shear rate γ that, for a uni-directional velocity gradient, can be expressed as:

$$\gamma = \frac{dv_y}{dx} \tag{2.12}$$

With v_y being the velocity profile between two adjacent posts. In this situation the shear is maximum at zero-distance from the post and it is expressed as:

$$\gamma = 4\frac{v_{max}}{G} \tag{2.13}$$

This equation is obtained by Davis after the determination of the fluid velocity profile between posts [38]. Considering the same maximum velocity of $2mm/s$ as before and a gap of $20\mu m$ the shear rate is equal to $\gamma = 200s^{-1}$ and the shear stress $\tau = 0.2Pa$ that according to literature [39] is similar to what experienced by blood in principal arteries and so completely harmless.

2.1.2 DLD design principle

In this paragraph, the main features characterizing a DLD array are discussed. Then, the explanation of how to use these parameters to design a device for sorting cells with different diameter is provided. The main parameters of a DLD array are post shape, size D_p, gap G, center-center distance between two adjacent posts $\lambda = D_p + G$, and the shifting distance between a row and its subsequent $\Delta\lambda$. (Figure 7[a]) This last parameter can also be represented as the tilting angle of the rows θ. After N columns of posts the lateral position of posts at column $N + 1$ is the same as in column one. N is called period.

$$N = \frac{\lambda}{\Delta\lambda} \tag{2.14}$$

The relation linking all these parameters is:

$$\lambda \tan\theta = \frac{\lambda}{N} \; or \; \tan\theta = \frac{1}{N} = \epsilon \tag{2.15}$$

ϵ is the row shift fraction, another strong designing parameter that has been frequently used in DLD literature [40]. As mentioned before, a particle of a given size will either stay or change lamina depending on the width of the streamline closest to the post. Inglis et al. calls this parameter β and exposes the previous theory with the following formulation [40]:

$$D_C = 2\beta \tag{2.16}$$

Where D_C is the critical diameter of the DLD. Anyway, the width of streamlines through the channel is not the same. Assuming constant the flow rate transported by each streamline its width depends by the parabolic distribution of velocity between two posts. The previous expression can be now related to the main features of the DLD:

$$D_C = 2\alpha G\epsilon \tag{2.17}$$

In this equation proposed by Inglis et al.[40] the width of the first lamina depends on the posts gap and the row shift factor, introducing a dimensionless parameter α to compensate for the parabolic velocity profile. As demonstrated by Beech in this case $\alpha = \sqrt{\frac{N}{3}}$ [41].

Another empirical formula was derived by Davis after testing more than 20 different design, modifying spherical particle size, gap and row shift factor for parabolic flow profiles: [38]

$$D_C = 1.4G\epsilon^{0.48} \tag{2.18}$$

The effect of different post shapes has been investigated in literature, but for our purpose the circular post shape worked best, having areas of zero flow where trapping is facilitated [37]. So, the effect of post shape is not considered in this thesis.

2.2 DEP theory

DEP is the physical phenomenon for which a nonuniform AC or DC electric field can induce in an uncharged particle or cells a movement due to the difference in dielectric properties of particle itself and the buffer in which it is immerged. It was firstly investigated in 1960s

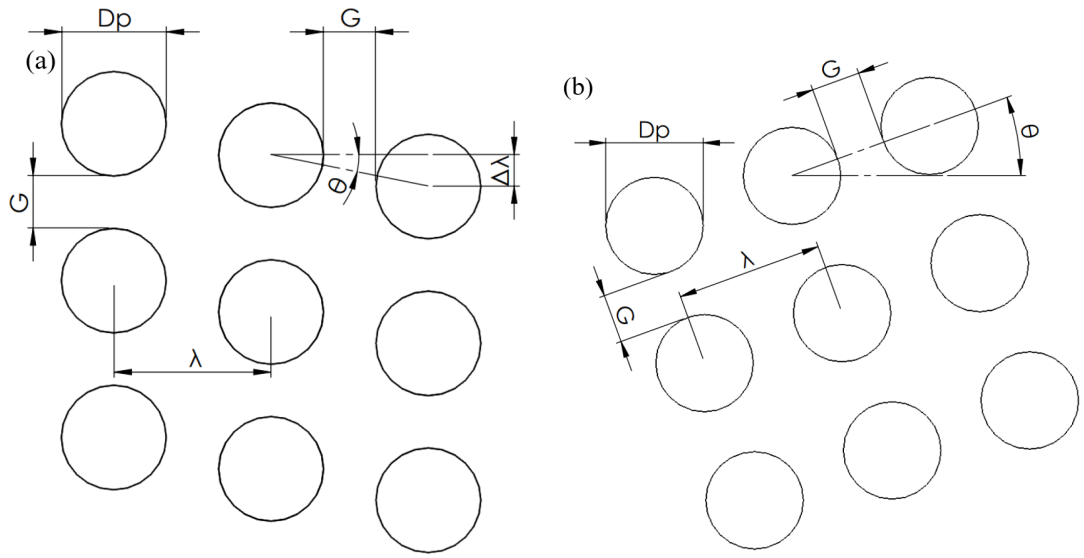

(a) Array perpendicular to the flow with tilted rows at a constant angle θ

(b) Rectangular array tilted with respect to the flow coming horizontally

Figure 7: DLD design parameters.

by Pohl [42] and then widely utilized in microfluidics as an active sorting method for cells characterization and isolation [43].

The DEP force is expressed as:

$$F_{DEP} = 2\pi\epsilon_0\epsilon_r r^3 Re(f_{CM}) \cdot \nabla \left|E_{(x,y)}\right|^2 \tag{2.19}$$

Where ϵ_0 $\epsilon_r = \epsilon_m$ is the permittivity of the buffer or medium used, r is the radius of the particle/cell $\nabla \left|E_{(x,y)}\right|^2$ is the gradient of the squared local electric field and $Re(f_{CM})$ is the real part of the so-called Clausis-Mossotti factor. The Clausis-Mossotti factor is a dimensionless

number that describes the how particles or cells react to the electric field applied. It depends by the dielectric properties of particles and buffer and is expressed as:

$$f_{CM} = \frac{\epsilon_p^* - \epsilon_m^*}{\epsilon_p^* + 2\epsilon_m^*} \tag{2.20}$$

With ϵ_p^* and ϵ_m^* being the complex permittivity of respectively the particle and the medium, also called buffer. They are defined as $\epsilon^* = \epsilon - j\sigma/\omega$ with ϵ permittivity, σ conductivity and ω angular frequency of the field $\omega = 2\pi f$. These simplified formulations can be used for polystyrene beads with a simple solid spherical shape but are not representative of the more complex cell structure. In fact, cells can be considered single-shell spheres, with a round core of radius r_c made of cytoplasm and a thin shell constituted by the cell membrane or thickness $r - r_c$. Morgan and Green described the ϵ_{Cell}^* for this complex shape with the equation [44]:

$$\epsilon_{Cell}^* = \epsilon_{Cyt}^* \left[\frac{\left(\frac{r_c}{r}\right)^3 + 2\left(\frac{\epsilon_{mem}^* - \epsilon_{Cyt}^*}{\epsilon_{mem}^* + 2\epsilon_{Cyt}^*}\right)}{\left(\frac{r_c}{r}\right)^3 - \left(\frac{\epsilon_{mem}^* - \epsilon_{Cyt}^*}{\epsilon_{mem}^* + 2\epsilon_{Cyt}^*}\right)} \right] \tag{2.21}$$

In this equation ϵ_{Cyt}^* and ϵ_{mem}^* are respectively the complex permittivity of cytoplasm and membrane of cells.

The Clausis-Mossotti factor is a complex constant, but its real part ranges from -0.5 to 1.0 depending on the dielectric properties of particles and medium. When the medium is more polarizable then the particle, then the real part of Clausius-Mossotti factor is negative resulting in negative DEP (nDEP). In this situation the particle will experience a force directed from areas of high field toward ones of low field. On the contrary, if the medium is less

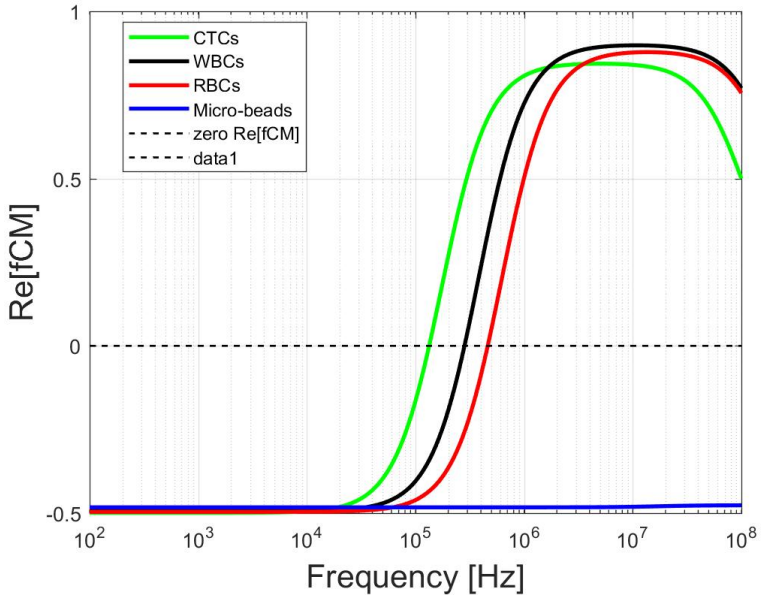

Figure 8: Real part of Clausius-Mossotti factor for different frequencies for white blood cells (WBCs), red blood cells (RBCs), circulating tumor cells (CTCs) and $10\mu m$ polystyrene microbeads.

polarizable, then the particle experiences positive DEP (pDEP), Clausis-Mossotti factor is positive and di-electrophoretic force pushes the particle toward regions where electric field is stronger.Differences in $Re(f_{CM})$ for blood cells are used in this work to target specifically WBCs. In fact, by tuning the frequency of the applied AC field it is possible to selectively act on particles with different dielectric properties, exploiting either positive or negative DEP. In Figure 8 the variation of $Re(f_{CM})$ with frequency is presented for the different cells considered. The conductivity of the medium σ has been set to $120\mu S/cm$ with a relative permittivity ϵ_r of 80. Dielectric properties of particles and cells have been found in literature [43].

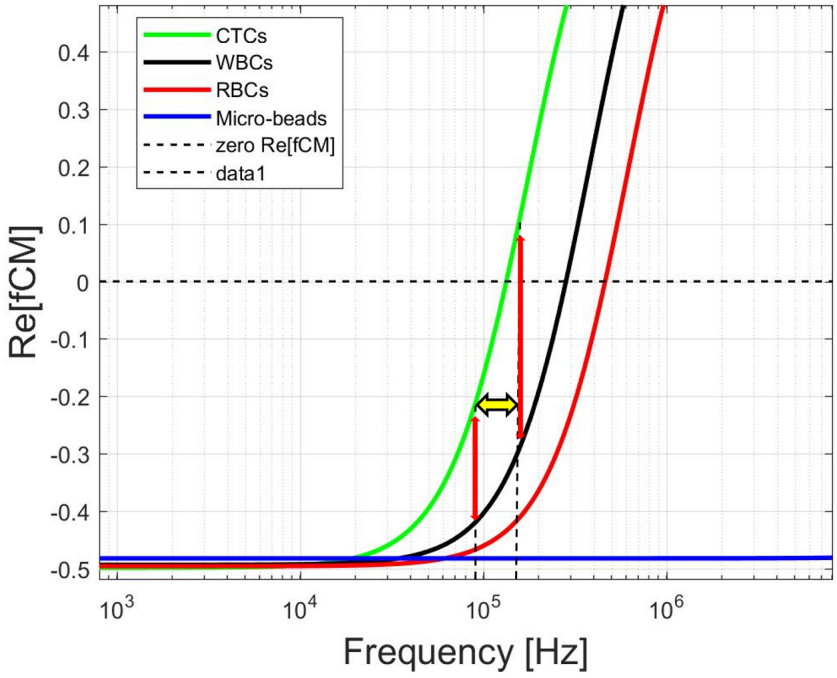

Figure 9: Detail of $Re(f_{CM})$ of different cells and particles between 10^3 and 10^7 Hz.

From graph in Figure 9 it is possible to see how WBCs and CTCs experience a different DEP force in a wide range of frequencies ($10^4 \div 10^6$). The red arrows show the difference in Clausius-Mossotti factor between CTCs and WBCs in a range of frequency highlighted by the thick yellow arrow ($9 \cdot 10^4 - 2 \cdot 10^5 Hz$). At the same time, it is evident how the behavior of WBCs and $10\mu m$ polystyrene microbeads is similar for frequencies below $10^5 Hz$. Based on the dielectric affinities of these different particles the decision to test the device potentialities with microbeads has been taken, since polystyrene particles $Re(f_{CM})$ has the same value as WBCs, RBCs and CTCs one at relatively low frequencies. This choice has been made to reduce costs, time and complexity of the experiments, still providing significant results.

For applications in frequencies below $50kHz$ the negative DEP force experienced by microbeads mimics the cells behavior under an AC field. In particular, at $50kHz$ the real part of Clausius-Mossotti factor differs of an appreciable 0.1 between microbeads (mimicking WBCs) and CTCs, permitting to selectively trap the beads and isolate CTCs.

2.2.1 Insulator-based DEP

In the proposed device the AC electric field is applied in the horizontal direction over the DLD array made of PDMS. This material is an insulator and so the field lines, when encountering non-conductive pillars, deviate to the region between two posts where conductive buffer is streamed. This creates non-uniformities through the array, resulting in areas where the field is stronger and in other where it is almost absent. This technique is called insulator based di-electrophoresis or iDEP. This solution addresses the fouling and bubble-formation problems of traditional DEP that, instead of insulating posts, exploits patterned electrodes at the bottom of the channel. On the other hand, the main drawback of this technique is the heat produced by the concentrated field between insulator obstacles due to Joule heating. Although, iDEP has been proved to be a reliable and effective solution for cells, bacteria and micro biological particles trapping [46].

2.2.2 Electric-field simulation

Simple simulations were run to better understand the effect of the electric field over different designs. The simulations were performed using COMSOL Multiphysics 3.2, solving the Laplace equation over a small domain of four pillars representative of the array:

$$-\nabla \cdot (\epsilon_0 \epsilon_r \nabla V) = 0 \tag{2.22}$$

Where V is the potential applied, $\epsilon_O = 8.854 \cdot 10^{-}12 F m^{-1}$, ϵ_r is the relative permittivity (80 for water, 2.5 for PDMS). An AC electric field of frequency $1kHz$ was simulated for the four different designs. The average intensity of the field imposed in the model was of $50V_{rms}/mm$ corresponding to a total difference of potential of $600V_{rms}$ between the two electrodes. The electric field is directed horizontally as the flow. Figure 10 displays the electric field in design 1 geometry. On the left it is possible to see a simulation of the horizontal electric field. The average field simulated was of $50V/mm$, corresponding to an overall difference of potential of $600V_{rms}$ between the two electrodes. The image shows effectively how the insulating posts concentrate the field up to a value of $80V/mm$ between the pillars, while the areas behind PDMS pillars are almost completely insulated. On the right the electric potential is represented in mJ. The white arrows show in a logarithmic scale the direction and intensity of the negative DEP force acting on $10\mu m$ particles with a Clausius-Mossotti factor of -0.49. The same results of simulations for design 2, 3 and 4 are displayed in Figure 11.

2.3 A balance of forces

In this paragraph an analytical explanation of particle trapping in DLD array is given and some images from experiments are provided to show and demonstrate this phenomenon. A balance of forces acting on microbeads flowing in the device is presented, starting with some assumption regarding the flow and the particles. First, because of the low Reynolds number, particles are moved by a creeping flow. Second, thermal and electrostatic effects on particles

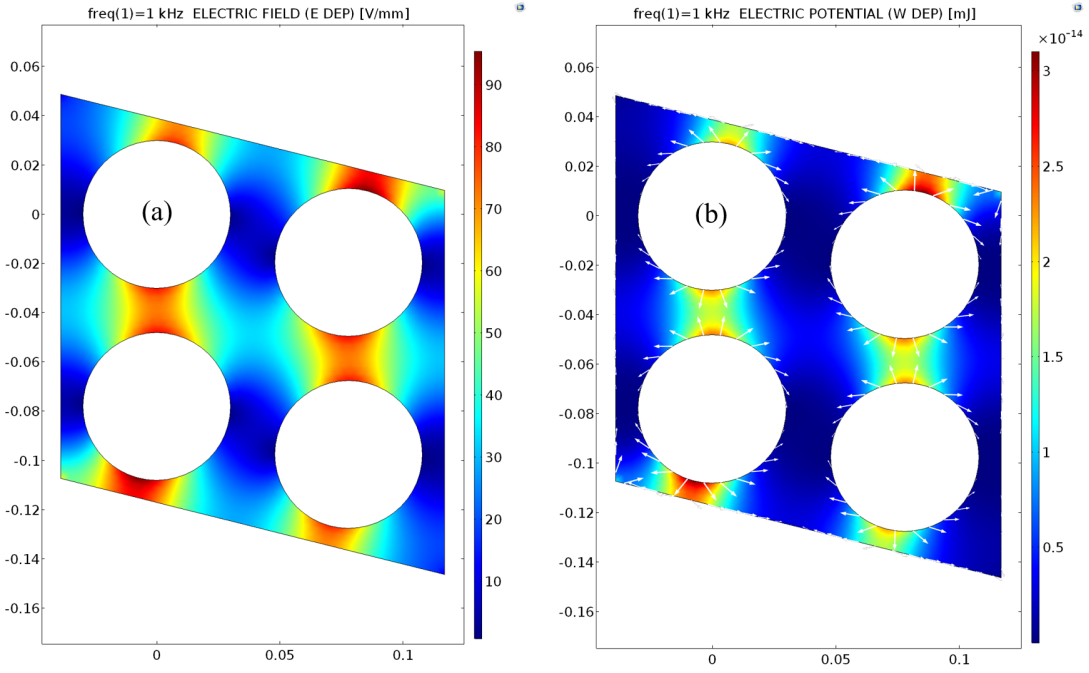

Figure 10: $1kHz$ AC Electric field and electric potential for Design 1 array.

and flow are negligible. Third, particle size has no effect on both flow and electric field. Finally, the effect of channel height on the electric field is negligible. Given a creeping flow the viscous force transporting particles can be calculated with the Stokes law and depends directly on the difference between flow and particle velocity:

$$F_{drag} = 6\pi\eta r(u_p - u_{flow}) \tag{2.23}$$

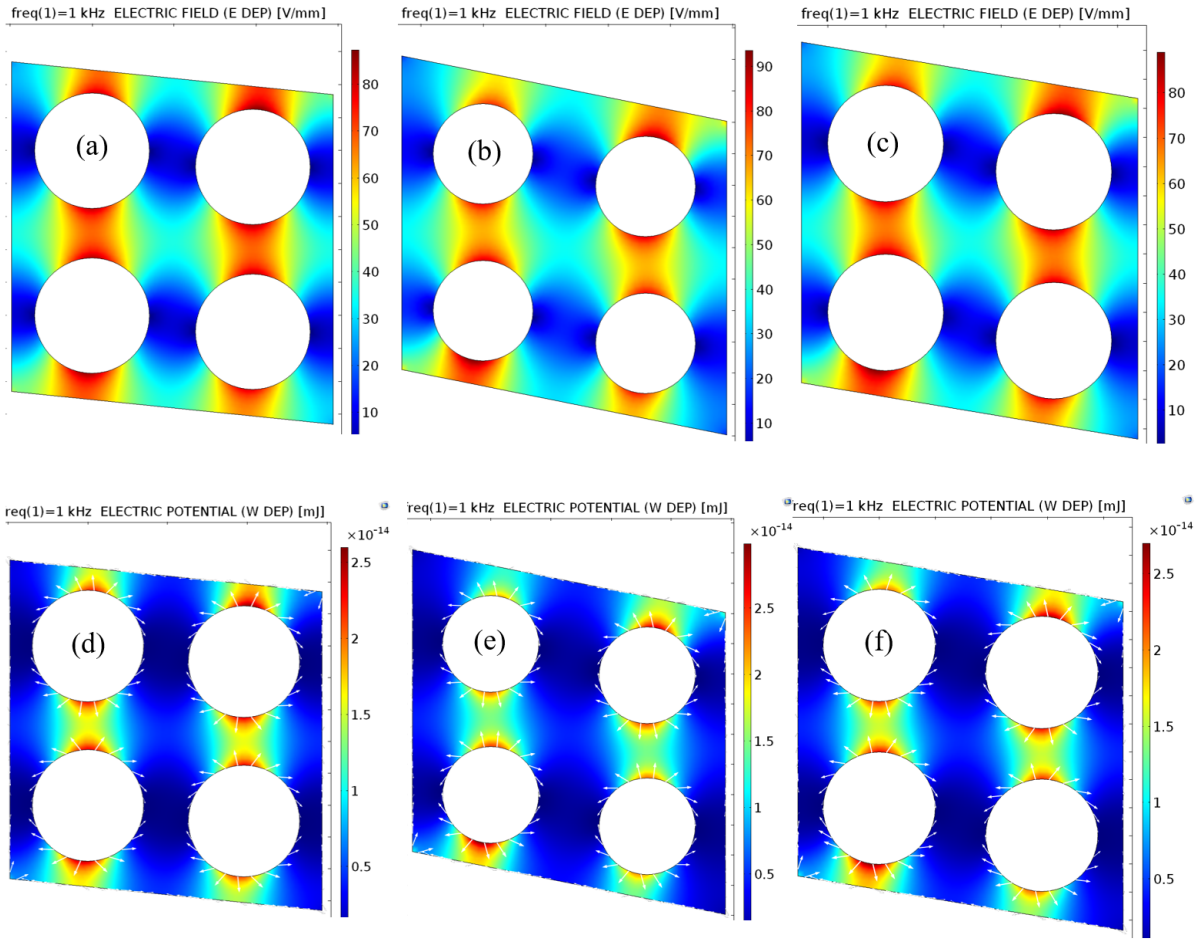

Figure 11: Electric field and potential for design 2-3-4.

The other major force acting on particles is the negative DEP force induced by non-uniformities obtained in the electric field by insulating pillars. As presented before in Equation 2.19 this force is expressed as:

$$F_{DEP} = 2\pi\epsilon_0\epsilon_r r^3 Re(f_{CM}) \cdot \nabla \left|E_{(x,y)}\right|^2 \tag{2.24}$$

The sequence of a particle moving through the array when the electric field is applied is showed in Figure 13, this motion can be discussed considering the DEP force graphs presented in Figure 11 (d). In Figure 13-(a) the particle is travelling through the narrow corridor between 2 posts. In this situation the nDEP force is exerted perpendicularly to the particle motion, having no influence on its velocity. Following the streamline, the bead approaches the pillar in Figure 13-(b) and Figure 12-(c). At this point the force exerted by nDEP overcomes Stokes force, moving the particle toward the lower electric potential region and eventually trapping it Figure 12-(d). Given that normal forces are balanced a focus is made on the tangential component, when in equilibrium it is:

$$F_{drag_t} = 6\pi\eta r(u_p - u_{flow}) = F_{DEP_t} \tag{2.25}$$

It is interesting to observe that, as the particle slow down, if the flow has a constant velocity, the viscous force should increase. Although in the observed case, the fluid slows down from the narrowing between two pillars to the wide area immediately after due to the increase in section area. Moreover, when the particle moves around the post, either because moving in zig-zag mode or being displaced by the nDEP force, it experiences a zone where the flow field is almost null. In Figure 12 a qualitative force balance of the trapped particle moving to equilibrium position is provided.

Depending on its dimension and the DLD array angle a particle can experience a reaction force when bouncing on pillars, this force will be normal to the post radius and directed from

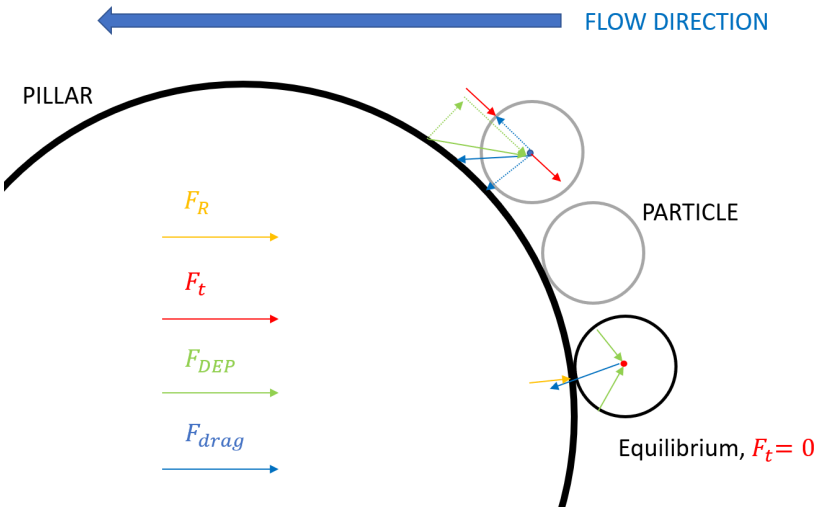

Figure 12: Scheme of forces acting on the particle during the trapping process. F_t, in red, is the resulting tangential component, F_R, in yellow, is the normal reaction of the pillar.

its center to the particle one. Assuming a completely inelastic hurt, the particle speed after the collision is reduced only to the component tangential to pillar circumference at contact point. This situation is similar to the one detailed in Figure 12 and explained before, immediately after the collision forces directed normally to post radius are balanced while on the tangential plane the nDEP force acting on the particle overcomes the Stokes force, trapping it either against or in between pillars until the electric tension is turned off.

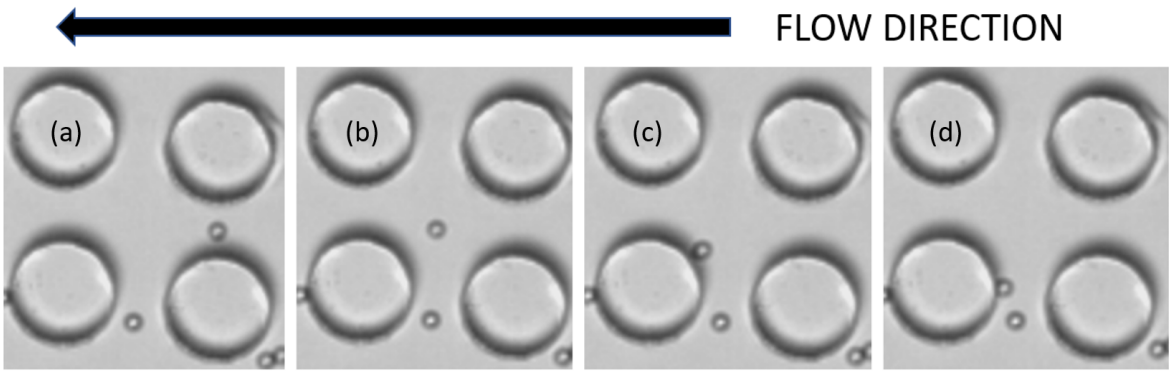

Figure 13: Sequence of images showing the particle motion and then its trapping when an AC electric field is applied.

2.4 Design

The design process started from the analysis of what done previously by other researching teams [3], then implementing different solutions to test the effectiveness of the concept and improve performances. The result is 4 designs with different array characteristics to explore the influence of DLD design parameters on trapping. They all present the same structure, developed after several trials to respond to fabrication and set-up issues. Figure 14-(a) shows microchannel details, S indicates the series of slots used at both inlet and outlet to straighten the flow before particles enter the array. P is the post array, it is possible to appreciate the inclination of rows of pillars through the device. Figure 14-(b) displays an outlook of the complete device with all features. A and B are respectively the sample and sheath flow inlet, C

are the outlets, D the electrodes reservoirs and E are used to vent the pressure in the electrode channel and remove bubbles from the device.

In the following table it is possible to see the parameters used for the DLD array of the different designs.

TABLE I: DESIGN CHARACTERISTICS COMPARED

DESIGN		**D1**	**D2**	**D3**	**D4**
Post Diameter	μm	60	70	32	40
Postgap	μm	18	28	20	18
Angle	deg	14	5.71	11.47	9.54
N		4.0	10.0	5.0	6.0
Gap/Diameter ratio		0.3	0.4	0.6	0.5
DLD Critical Diameter					
Analitical	μm	10.4	10.2	10.4	8.5
Davis	μm	12.9	13.0	13.0	10.7
Average	μm	11.7	11.6	11.7	9.6

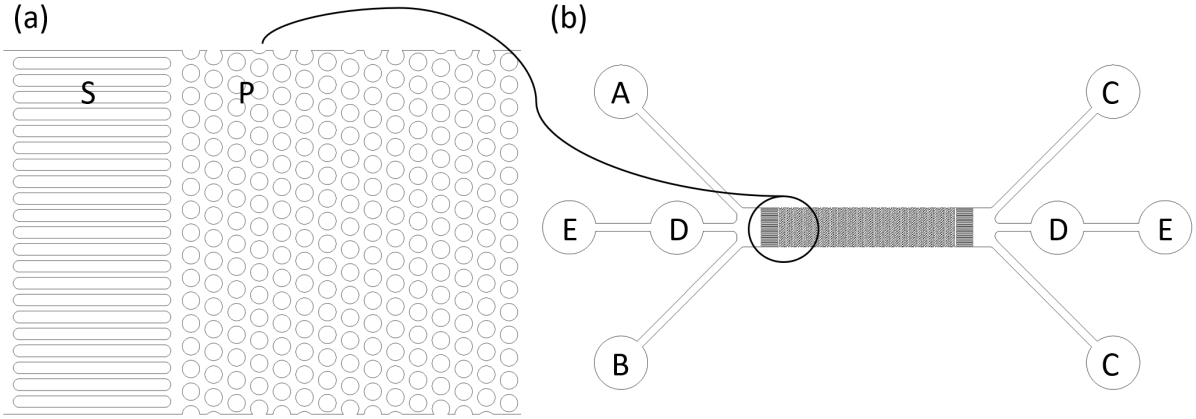

Figure 14: Schematic images of the design structure.

2.5 Fabrication

Fabrication was made following PDMS soft-lithography. The device consists of a poly-dimethylsiloxane (PDMS) layer where the 3D design was printed attached to a glass slide. Multiple copies of a PDMS device can be made by creating a mold. The mold was made by SU-8 photolithography over a silicon wafer. All the steps of fabrication after the CAD design preparation are now presented.

When the drawing of the chosen design was ready a .DXF version of the CAD file was prepared including others information needed and then sent to the vendor for mask printing. The designs are printed over transparent plastic sheets using a dark color. When exposed to UV light only the transparent areas will let the light pass through the mask, hardening the

photoresist and transferring the design onto a 4-inches silicon wafer. This procedure is called photolithography and is made into a clean room, where the atmosphere is regulated by filters and the content of dust and suspensions in the air is drastically reduced. In this case these procedures were made in the Nanotechnology Core Facility (NCF) of UIC, situated at the third floor of the Engineering Research Facility (ERF).

First, the 4-inches silicon wafer was immerged in acetone for 30 seconds, then in IPA for other 30 seconds. Then, dried the wafer with compressed air, it was left for few minutes on a heated plate set at 100 $°C$ to evaporate all the IPA. The wafer was then placed on the spin coater and centered. The photoresist used for this procedure was SU-8 2050 [see appendix for technical sheet]. It was disposed from the initial container to a smaller one to simplify the pouring and reduce the accumulation of impurities on the sides of the bottle. Then the photoresist was poured onto the center of the wafer until 2/3 of its surface was covered. The spin coater was set to $500rpm$ for 5 seconds at the beginning and then ramped up to $3000rpm$ in less then 5 seconds, maintaining this speed for 30 seconds. This as indicated by the technical sheet of the photoresist to obtain a layer height of $40\mu m$ [**?**]. Before pre-curing, the excess of resin on the edge of the wafer accumulated due to spin coating was removed manually with a napkin. The photoresist was pre-cured at 70 $°C$ for 2 minutes and then $100°C$ for 7 minutes, finally placed on a napkin to cool it down. In the meanwhile, the mask was prepared. Since we used a thin plastic mask we needed to cut it and attach it to a clean glass before inserting it into a Karl Suss MA-6 mask aligner. The Mask Aligner is a complex machine used to align the mask and the substrate before exposing it to UV light. In our case the alignment was

not needed since the design is composed of a single layer with constant height of $40\mu m$. The substrate has been exposed to a $19.5mW/cm^2$ power mercury light for 15 seconds, adsorbing a total energy of almost $300mJ/cm^2$. After exposure the wafer passes a post-curing process, before at $70°C$ for 2 minutes then at $100°C$ for 7 minutes. During this curing the exposed structure should become visible, otherwise it means that the SU-8 has been under-exposed. Let cool down the wafer on a napkin and then immerged it into the SU-8 developer in two steps for a total developing time of 20 minutes. To improve the strength of the SU-8 structure and anneal microcracks a post-baking cycle was done, ramping up and down slowly between $70°C$ and $160°C$. The obtained mold has been silanized to facilitate the removal of PDMS after casting. Silanization is done by leaving the mold for 5-7 hours under vacuum with few drops of a silanizing agent as perfluorooctyltrichlorosilane in an aluminum cap next to it. The agent will deposit a thin hydrophobic film of alkoxysilane [52] .

PDMS is prepared by mixing 25 grams of part A of sylgard 184 with his part B in a 1:10 ratio. The mixture was stirred for up to 3 minutes to obtain a perfect mixing of the 2 components, then it was slowly poured onto the mold. The mold filled with PDMS was then degassed into a vacuum bell for 20 minutes to remove bubbles and baked at $75°C$ for 50-60 minutes to cure the PDMS. Once ready the PDMS replica was gently demolded and placed on a mat to cut the edges and punch the holes for inlets, outlets and electrodes using a $1.5mm$ puncher. Finally, the PDMS was bonded with a 3 x 2 inches glass slide previously cleaned with methanol and IPA. The bonding was made using a Harrik Barrel Plasma Etcher in the clean room, setting the pressure to 350 $mTorr$ in O_2 atmosphere and igniting the electric arc at Hi

power for 40 seconds. A curing at $75°C$ over night followed the etching to increase the strength of the bonding and permit the device to sustain high pressures.

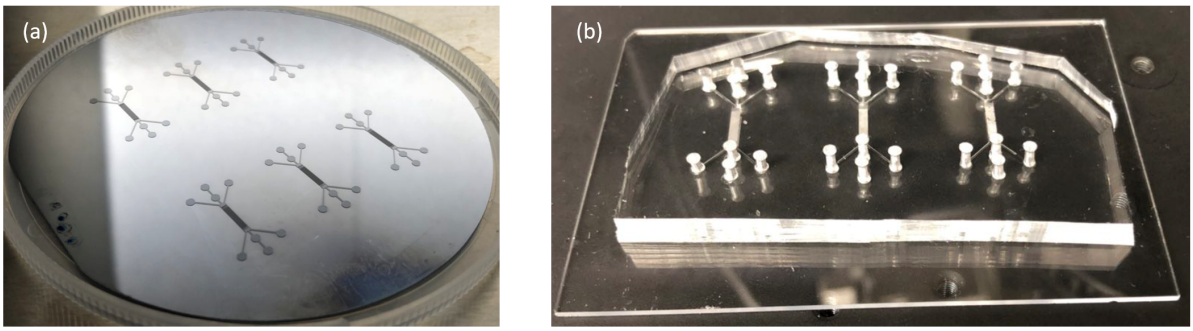

Figure 15: Mold(a), device(b)

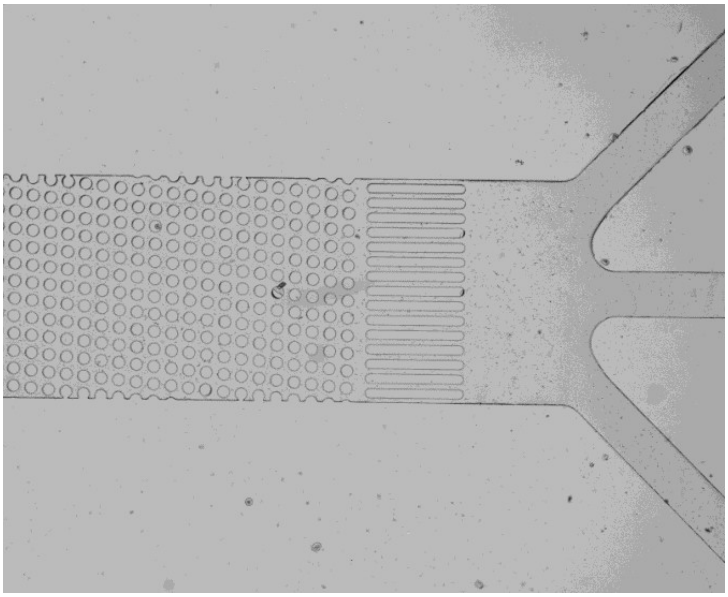

Figure 16: Microscope image of final PDMS device.

CHAPTER 3

EXPERIMENTAL SETUP

In this chapter the experimental set-up is presented together with cells sub culturing procedure and buffers characteristics. The showed set-up is the end of an optimization process of instruments and methods to obtain the most reliable and replicable results in experiments. All the images and videos were recorded using an inverted Nikon Eclipse Ti-S microscope connected to a Canon high-speed camera used to slow-down images and analyze the flow. The camera used has no color resolution, so to make possible to distinguish cells and microbeads the white top light of the microscope was combined with a blue bottom light generated with a X-Cite 120 LED.

3.1 Pump Set-up

To impose a flow through the device a syringe pump equipped with 2 BD plastic syringes with a total volume of $14.5ml$ was used. The syringes were solidly inserted into a Chemyx fusion 200 syringe pump. A luer lock plastic fitting was used to connect each syringe with a plastic tube of 1/8 inches OD and 1/16 inches ID. The same pieces of tubing were used at the outlet and the outflow was collected in a becker.

The tubes were directly connected to the device inlets and outlets by the $1.5mm$ holes punched during device fabrication. In the same way the 30 18G blunt needles used as electrodes were inserted into their reservoir. Sometimes the needle outer diameter ($1.27mm$) was not thick

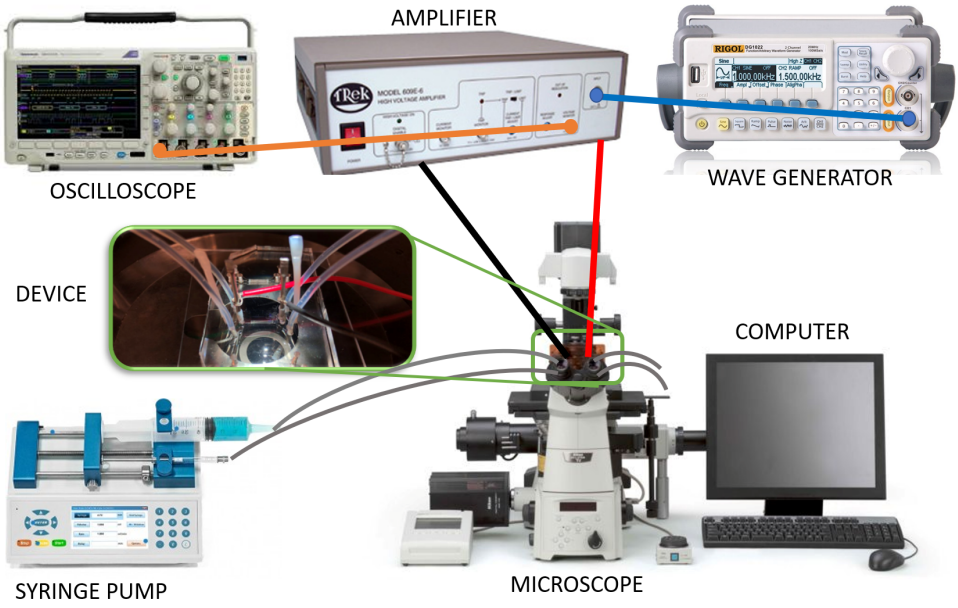

Figure 17: Scheme of the complete experimental set-up.

enough to fit the punched hole in the device, causing leakages. The problem has been solved by wrapping the tip of the needle with tape, enlarging its size and ensuring a connection strong enough to resist imposed pressures.

After the device is fully connected a high flow rate (or pressure) is imposed, to fill completely the DLD array and remove all the air bubbles present in the device. Usually a pressure of $500mBar$ for a minute was enough to completely fill the device with the sample. The sample was connected to the bottom inlet of the device, while a sheath buffer was pumped to the top inlet. With bottom inlet is meant the inlet channel facing the side of the device where the DLD array is tilted in the direction on the other side of the device, the top inlet side. Figure 20

Figure 18: Syringe pump equipped with 2 BD syringes.

This configuration permits to exploit DLD separation for particle of different size, having the bigger ones moving according to the array angle to the other side of the device (bottom to top) and the smaller one following the flow without changing side. The isolated position of the electrode permits to exploit strong electric fields without harming the cells flowing through the array and avoiding the formation of bubbles in the main channel. Finally, the vent channel prevents the formation of air bubbles and makes possible the removal of dirt and further bubbles due to Joule effect.

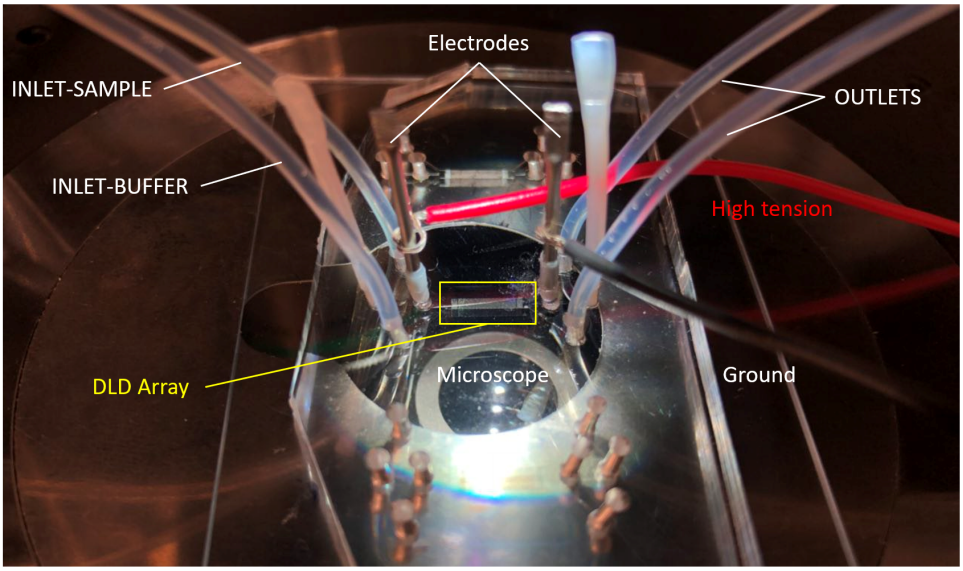

Figure 19: Device connections in experimental set-up.

3.2 Electrical set up

The electric field was created imposing a difference of potential at the electrodes. The alternate current (AC) tension was imposed using a RIGOL DG1022U functional arbitrary waveform generator. This device can produce an AC tension with an intensity up to $20V_{pp}$ (Volts peak to peak) and a maximum frequency of $25MHz$. To achieve an higher intesity of the field the signal coming from the wave generator was amplified using a T-REK 609E-6 Tension amplifier. This amplifier amplifies the input tension for a 1000 times factor, with an output maximum limit of $4000V_{rms}$. A Tektronics TDS 3054 oscilloscope was connected to the amplifier to monitor the waveform signal. In experiments a simple sine wave with zero phase was generated.

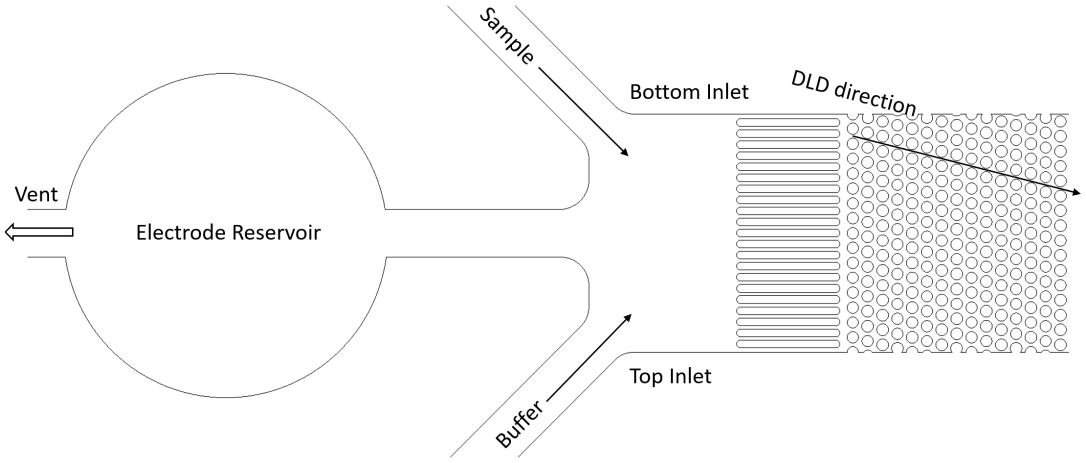

Figure 20: Device connections and visual definition of top and bottom inlet

After connecting all these instruments together, the wave generator and the tension amplifier were turned ON carefully. Then the high voltage and ground wires were connected to the electrodes, wrapping the wires around the blunt needles. The needles were fitted in the device reservoir connected with the main channel, the distance between the electrodes was of $12,12mm$. A frequency of $1kHz$ and a small tension of $100mV_{rms}$ was set on the wave generator, resulting in a tension drop of $100V_{rms}$ through the device. The signal was sent from the wave generator to the device by pushing the output button of the channel connected with the amplifier. From this point the tension was increased to the desired value, always being aware of the surroundings and taking precautions from dangers linked to high voltages.

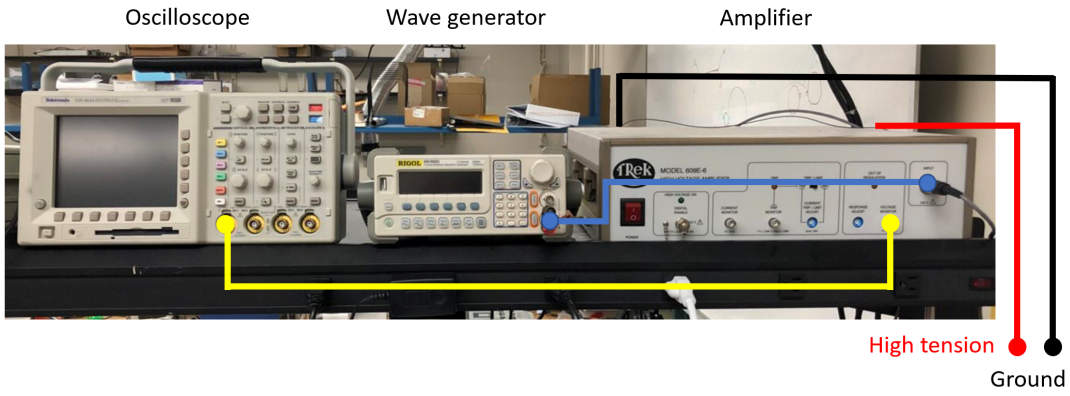

Figure 21: Electrical Set-up.

3.3 Particles and buffers

Experiments were run using polystyrene microparticles and A549 line adenocarcinoma metastatic cells. Two different microbeads were used for these experiments, $9.9\mu m$ and $4.8\mu m$ Fluorescent beads from producer Sigma-Aldrich.

For experiments with microbeads a 0.1 x TBE buffer was prepared by diluting 10 x TBE with DI water. Then, 0.05% (w/v) Sodium Dodecyl Sulfate (SDS) was added to the buffer to reduce particles adhesion to pillars and slots in the device. The conductivity of the buffer was measured with a TDS meter and then converted in $\mu m/Sm$. A Azzota pH-meter was used to evaluate the pH, the probe has been immerged in the buffer for 20 minutes before the reading. The prepared buffer resulted to have a conductivity σ of $280\mu S/cm$ and a pH of 8.65.

Cells were suspended in a DEP buffer based on DI water with 8.5% sucrose (w/v), 0.3% dextrose (w/v) and 0.725% (v/v) DMEM.[47] The conductivity and pH of this buffer were measured respectively as $120\mu S/cm$ and 6.78.

3.4 Cells

A549 is an adenocarcinoma cell line isolated in 1972 from a lung cancerous mass removed from a 58-year-old Caucasian male [48]. Cells were received already thawed in a T-75 flask, then immediately sub cultured in T-25 flasks and kept into an incubator where the environment was controlled, maintaining a temperature of $37°C$ and a CO_2 level of 5%. All the procedures [49] involving cells were done inside a Class II, type A2 Biosafety cabinet to avoid contamination of the sample with bacteria and to prevent any risk of disease transmission to researchers.

3.4.1 Sub culturing

Firstly, $500ml$ of medium was prepared with this composition: 89% 1 x DMEM/F-12 50/50 with L-glutamine and 15mM HEPES, 10% FBS (fetal bovine serum), 1% PSN, composed by $50\mu g/ml$ Penicillin, $50\mu g/ml$ Streptomycin, $100\mu g/ml$ Neomycin; then stored in a fridge at $5°C$.

When a confluency of 70-80% was reached cells were sub cultured, usually this occurred every 3-4 days. The medium was warmed up to $37°C$. In the meanwhile, cells were taken out of the incubator and the cell culture medium was discarded using a pipette. Then, cells were rinsed using $5ml$ of PBS (saline phosphate buffer) and pipetting gently to wash away the old medium. After this, $1ml$ of Trypsin-EDTA 0.05% was added to the T-25 flask to detach cells from the bottom. The flask was placed again at $37°C$ in the incubator for 5 minutes. Once

cells were detached Trypsin was deactivated by adding $3ml$ of fresh cell culture medium. The flask was gently rinsed by pipetting 3-4 times to fully detach all cells from the bottom, then the suspension was placed into a $15ml$ conical tube. The suspension was centrifuged at $3000rpm$ for 5 minutes to collect cells at the bottom of the tube. Then, the supernatant was discarded, $2ml$ of fresh medium was added, pipetting gently 4-5 to mix the cells into the suspension and obtain a homogeneous concentration. Cells were counted using a hemocytometer to calculate the concentration, the procedure is presented in the next paragraph cells counting. To subculture properly, a final concentration of $2.5 \cdot ((10)^4) cells/ml$ in a total suspension volume of $7ml$ is required. The right amount of cell suspension and cell culture medium is evaluated with:

$$cell\ solution\ needed\ = \frac{desired\ final\ concentration\ -\ final\ flask\ volume}{hemocytometer\ concentration} \tag{3.1}$$

$$medium\ needed\ =\ final\ flask\ volume\ -\ cell\ solution\ needed \tag{3.2}$$

Finally, the suspension was transferred into a new T-25 flask and placed in the incubator.

3.4.2 Cell counting

Cell counting is made using a hemocytometer, a special glass slide with a grid designed where cells can be counted under a microscope. This procedure is used in this work not only to sub culture cells but to evaluate cells viability too. At first, $50\mu l$ of cell suspension were collected in a 500 Eppendorf tube. Rinsed the hemocytometer with DI water, dried with compressed air and placed a 1 x 1-inch glass slide over it. Then, $16\mu l$ of suspension was pipetted into each side

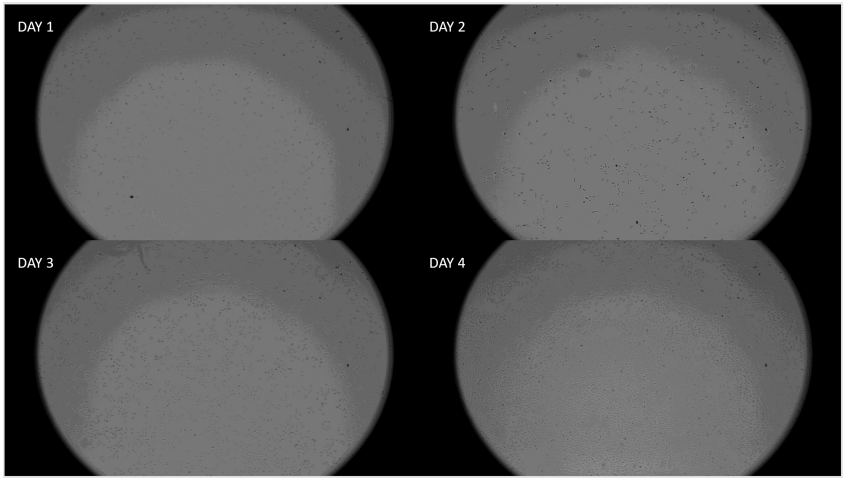

Figure 22: A549 cell culture growing.

of the hemocytometer. Cells were counted under a microscope, counting for both grids only the cells contained into the 4 corners of the grid. Finally, an average of cells count for every corner of the grid was calculated dividing by 8 the total number of cells in both grids. This number multiplied by 10^4 gives the concentration of the given cell suspension. If the suspension has been diluted before counting remember to multiply the value obtained before by a dilution factor given by the ratio between the total volume of suspension and the initial volume of cell suspension.

3.4.3 Sample preparation and viability calculation

For experiments the sample was prepared following the sub culturing procedure but suspending cells in the DEP buffer previously prepared instead that in the culture medium. After utilizing cells in experiments a viability evaluation is needed, the procedure is the following.

First, $50\mu l$ of cell suspension was mixed with the same amount of Trypan Blue 0.4% in a 500 Eppendorf tube. Then, the concentration of the solution was calculated with a hemocytometer as presented in paragraph 3.4.2, considering a dilution factor of 2. Trypan Blue is diazo dye and cell impermeable, when cells are alive the dye can not pass through the cell membrane and under the microscope the cell appears transparent as usual. Instead, the cell looks blue when dead, because its membrane becomes permeable to the coloring.

CHAPTER 4

RESULTS AND DISCUSSION

Results and parameters of all experiments are presented in this chapter, starting from devices characterization and ending with cells testing and viability, passing through the validation of the method proposed in the introduction using polystyrene particles and cancer cells. These results not only validate this novel technique for circulating tumor cells sorting, but also provide a comparison between different design and their performances, that will be better discussed in conclusions.

4.1 Polystyrene beads trapping

Trapping experiments and results for $9.9\mu m$ particles only are here presented. Tests were conducted for all the 4 designs imposing different values of flow rate and then increasing the tension applied to the device until trapping was obtained. Trapping was evaluated by analyzing 2 minutes long live videos of the particles exiting the array before and after an electric field was applied. When any particle flowed out of the DLD channel within the 2 minutes, then the tension imposed at that moment was registered as 100% trapping voltage. The tension was then slightly decreased until the first particle left the array, that level of tension was registered as an ideal 90% trapping voltage. The syringe pump set-up presented in paragraph 3.1 was used, particles were suspended in the 0.1 x TBE buffer (conductivity $280\mu S/cm$, $pH8.65$), experiment parameters and results are showed in Table II.

TABLE II: TRAPPING VOLTAGE VERSUS FLOW RATE FOR DIFFERENT DESIGNS AT $10kHz$ FREQUENCY.

	D1		**D2**		**D3**		**D4**	
Flow rate $[\mu L/min]$	$[V_{rms}]$ 90% **trap**	$[V_{rms}]$ 100% **trap**	$[V_{rms}]$ 90% **trap**	$[V_{rms}]$ 100% **trap**	$[V_{rms}]$ 90% **trap**	$[V_{rms}]$ 100% **trap**	$[V_{rms}]$ 90% **trap**	$[V_{rms}]$ 100% **trap**
0.5	700	720	730	750	730	750	690	720
0.7	720	740	740	760	740	760	740	770
0.9	800	820	750	770	750	770	860	890
1.1	870	920	890	950	810	830	970	1010

To avoid the risk of bubble formation and device break down the voltage had to be limited below $1700V_{rms}$. To do so, it was used a range of flow rate for which particles got trapped even at relatively low tensions. To better understand these results and compare design performance, in Figure 23 a line graph shows the dependence of electric field on flow rate to achieve 100% trapping. The value of the horizontal electric field has been obtained by dividing the total difference on tension in V_{rms} for the distance between the electrodes in mm.

From this graph it is possible to see that for low flow rate all the devices have a similar trapping capacity. But when it comes to trap particles moving in flows travelling over $1\mu l/min$ a dramatic difference is observed, with device 3 capable to achieve trapping exploiting a field 10 to $20V_{rms}/mm$ less intense than the others. Remembering the differences in the sectional area of these designs it is interesting to show the dependence of the trapping electric field on the fluid velocity Figure 24.

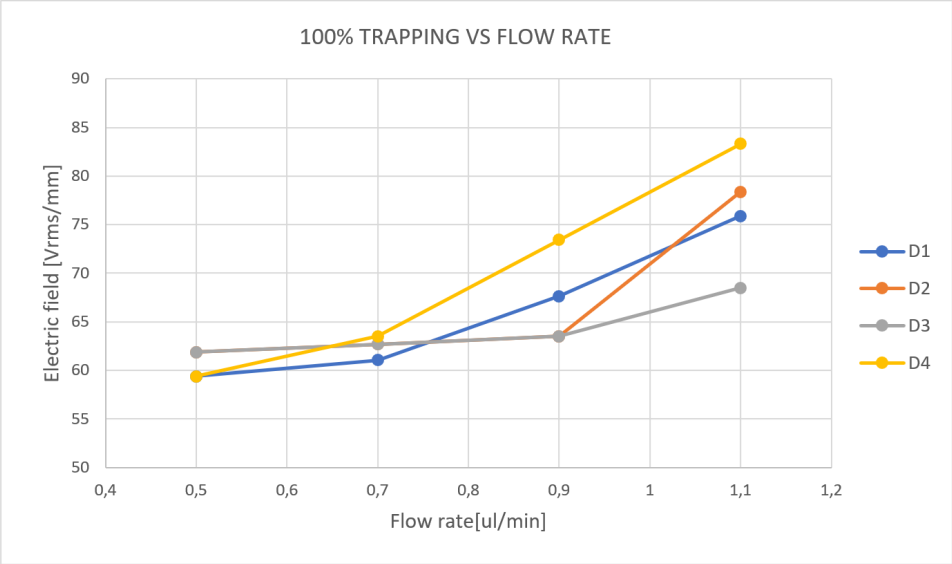

Figure 23: 100% particle trapping versus flow rate for different designs.

The fluid velocity is calculated for the minimum sectional area, the one in correspondence of a vertcial posts column. This graph does not really represent the conditions we have in the proximity of a pillar where trapping happens, but shows how the average fluid velocity is not an interesting parameter in the trapping phenomenon. A hint regarding this result was already given in the force balance paragraph where it was highlighted how trapping occurs in regions of null flow. On the other side the comparison between the real particle speed through the array and the electric field capable of trapping it can become useful to determine which design performs the best. This relation is presented in Figure 25, the average velocity of the particle was measured with ImageJ counting how many frames it took 20 particles to move between two determined positions in the array. In this graph results are similar for all the design, confirming

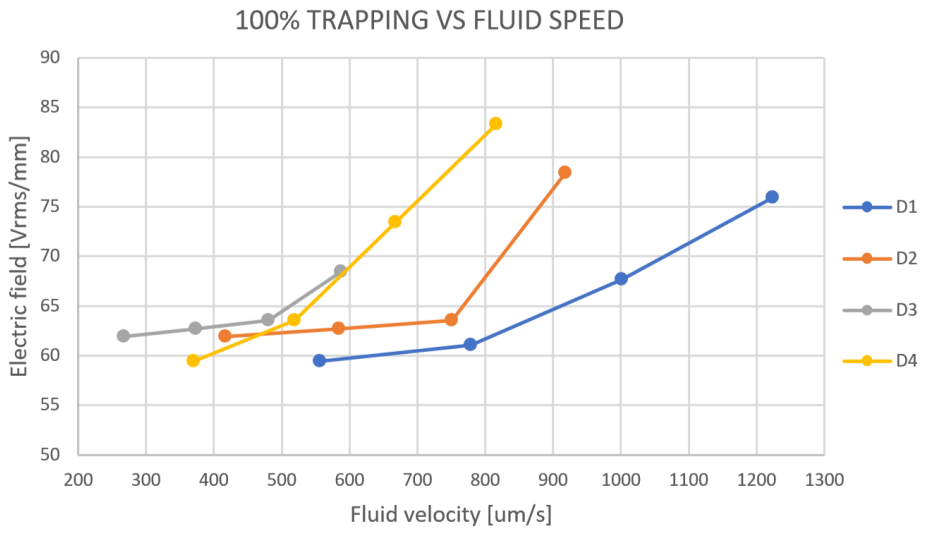

Figure 24: 100% particle trapping versus fluid velocity for different designs.

what supposed before. Design 1 makes an exception, being able to trap particles faster than in the others.

In Figure 26 it can be appreciated the trapping of microbeads around pillars of device 2 when a flow of $0.5\mu l/min$ is imposed and a horizontal AC electric field of intensity $70V_{rms}/mm$ is applied. It is interesting to observe from Figure 26 (a) that particles are moving around pillars in zig-zag mode as expected, given that the critical diameter of this design was estimated around $11.5\mu m$.

4.2 Polystyrene beads sorting

A sample with 4.8 and $9.9\mu m$ fluorescent polystyrene particles in 0.1 x TBE buffer was prepared to demonstrate that particles can be selectively trapped not only depending on their dielectric particle but on their size too. Ideally, this appears evident by the formulation of

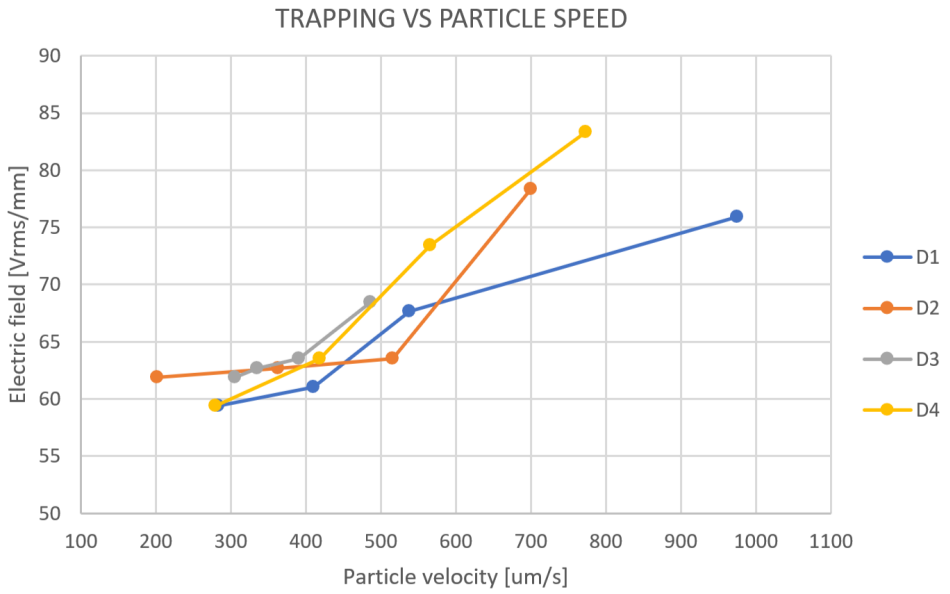

Figure 25: 100% particle trapping versus particle velocity for different designs.

DEP force, that is proportional to the cube of particle radius. Design 4 with a theoretical critical diameter of $9.5\mu m$ was used to run this experiment, expecting $9.9\mu m$ particles to move in bumped mode and the $4.8\mu m$ to move in zig-zag mode. All the other conditions are the same for the experiment presented in paragraph 4.1, the syringe pump set up was used to impose a constant flow rate of $0.5\mu l/min$, an AC tension of $900V_{rms}$ and $10kHz$ frequency was applied to the device. Results are presented in Figure 27, small particles are highlighted in green, big ones in red. It is evident how $9.9\mu m$ microbeads are trapped until the tension is switched off, while $4.8\mu m$ beads are never completely stopped by the electric field. Some smaller particles got trapped but this happened mainly because of the dirt and added obstacles that stopped bigger beads constituted to their motion through the array. Oppositely to what

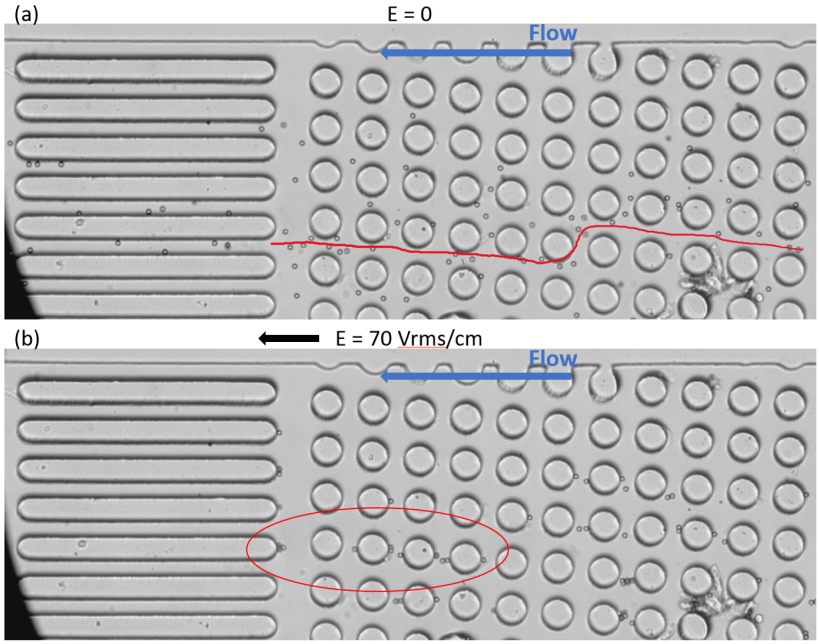

Figure 26: 9.9μm microbeads trapped applying an AC electric field.

expected, 9.9μm microbeads moved through the device in zig-zag mode as the other particles. This indicates to riconsider the formulation used to calculate the critical diameter of the DLD array, since it appers evident that in this case its real value is higher than 9.9μm.

4.3 Cells viability and throughput

Two important indicators to determine the feasibility of this separation method are cells viability and throughput. Viability indicates the percentage of survived cells after the sorting process that in this case involves them experiencing an intense electric field. Throughput, instead, is the percentage of cells passing successfully through the whole process, from sample preparation to collection. Cells were counted and then injected with a syringe pump into the

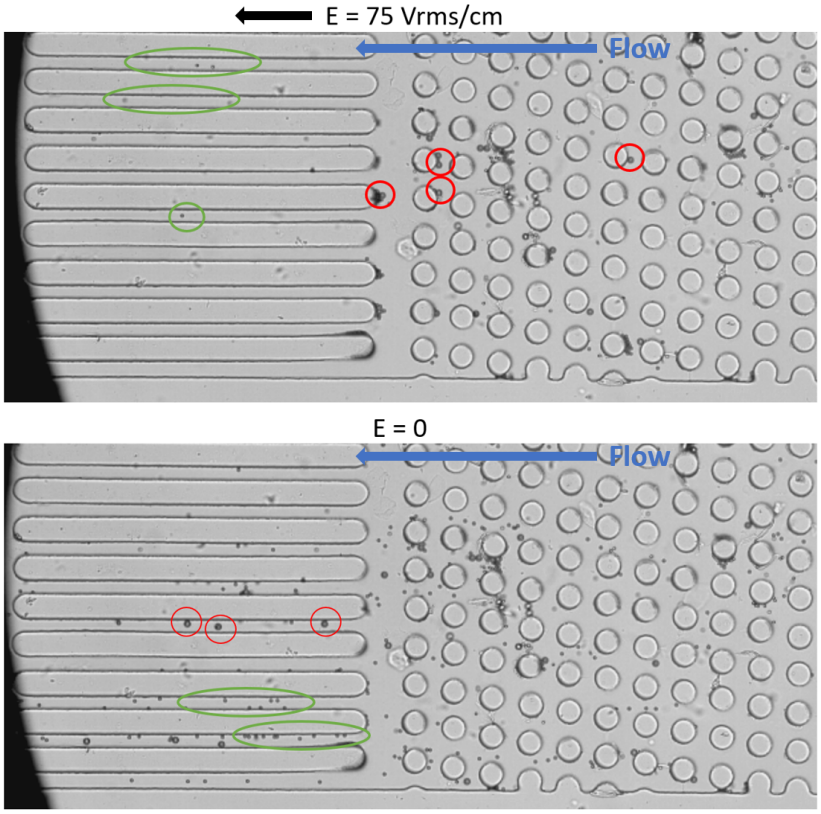

Figure 27: 4.8 and 9.9μm separated applying an AC electric field.

sample at a constant flow rate of 9.9$\mu l/min$ for 5 minutes. The process was repeated three times applying a voltage of 500,700 and 900 V_{rms}. Samples where collected at the outlet in a 500 eppendorf tube, and then counted as described in paragraph 3.4.2 cell counting, results are presented in Table III.

TABLE III: CELLS VIABILITY FOR DIFFERENT VOLTAGES

Voltage $[V_{rms}]$	500	700	900
Viability	90%	74%	68%

4.4 Cells and beads separation

An experimental run with polystyrene beads and A549 circulating tumor cells was done to demonstrate that selective trapping of particles with same size but different dielectric properties can be achieved. First, cells suspension was prepared starting from a sample at 90% confluency containing 10^6 cells. Then, the experimental sample was prepared mixing 4.8 and $9.9\mu m$ beads with cells suspension in its DEP buffer. The syringe pump set up was used to impose a constant flow rate of $0.5\mu l/min$, as for precedent runs. Once all bubbles were removed and the flow became stable an AC electric field was applied at a frequency of $10kHz$ and a tension of $500V_{rms}$. The field frequency and intensity was then tuned to trap 9.9μ m polystyrene beads, while cells and smaller particles flowed away to the outlet.

As stated before, the experiment was meant to show separation of particles and cells with same diameter and different dielectric properties. Anyway, as evident from Figure 28 the cells resulted to be bigger than $9.9\mu m$ beads. This implied that at 10kHz the difference in radius overcame the difference in $Re[f_{CM}]$, trapping CTCs at tension as low as $500V_{rms}$ for which microbeads were not trapped. To selectively trap $9.9\mu m$ polystyrene beads the frequency was

then tuned to higher values, but at $50kHz$ the voltage amplifier went out of regulation, unable to supply a tension above $350V_{rms}$. The obtained results is exactly inherent to what predicted and expected from theory, but the lack of better equipment prevented reaching the final goal of trapping particles while letting cells flowing out. From voltage amplifier datasheet the slew rate is $150V/\mu s$, the slew rate indicates the maximum speed at which an AC amplifier can move the voltage from one peak to the other. [**?**] This value is too low for the purpose of this experiment, since to make CTCs experience a 0 DEP force we need a frequency around 100 kHz, while the voltage to be applied to trap polystyrene beads resulted to be, from previous experiments, of at least 650 Vrms. This implies the use of a voltage amplifier featuring a slew rate up to $500V/\mu s$. Examples are model PD06087 and model 10/10B-HS from the same manufacturer T-REK, that come at a price below 10,000 $.

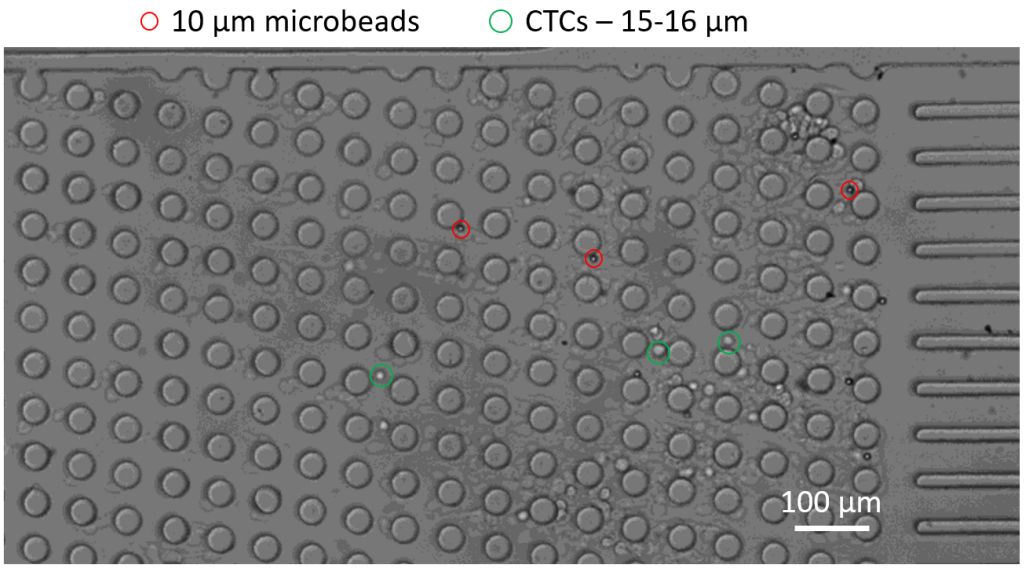

Figure 28: Cells and $10\mu m$ particles stuck in the DLD array.

CHAPTER 5

CONCLUSIONS AND OUTLOOK

In this thesis a novel method for label-free circulating tumor cells sorting is proposed. In Chapter 1 the tumor metastasis problem is presented together with an introduction on microfluidics separation. Later, a focus on microfluidics sorting is made, exposing working principle, advantages and drawbacks of different techniques. After introducing the concepts of DLD and DEP the idea of a novel solution is explained. Chapter 2 is divided in two parts, first showing the physics behind our concept, and then detailing the materials and fabrication method used. In Chapter 3 and 4 experimental set-up and results are presented and discussed. The final goal was to run these experiments to achieve, in the end, the separation of CTCs from whole blood samples. The collected tumor cells should be available not only for diagnostic but for analysis and specific drug development too. The choice to run experiments with polystyrene microbeads has been made to simplify the procedures, reduce the cost and try this sorting solution at an early stage. Nevertheless, the results obtained not only confirm our concept but encourage further tests of this method with blood cells and whole blood.

The critical issues of this proposal are here presented and discusses considering results from experiments to conclude that this technology has been proved to be feasible for the problem of CTCs sorting. Viability test showed a promising survival rate of 80% for the range of tension used in the experiments ($650 - 750V$). The number of WBCs that can be trapped in the array is limited but increasing the width and height of the device can solve this problem, providing

an array capable of trapping up to 10^6 cells. Trapped WBCs may influence the motion of other cells to a minor extend, but this does not affect CTCs travelling in bumped mode and so avoiding the obstacles created by WBCs in the region of slow flow between pillars. The designs used for experiments were chosen to simplify the fabrication and reduce the set-up time to perform more test of this concept. Modifications can be included to increase performances as throughput, flow rate and sorting efficiency by running more devices in parallel or increasing the main channel width and the number of inlets and outlets. From the comparison of different DLD arrays having similar critical diameter we can conclude that channels with narrower pillars can achieve a better trapping at the same flow rate, as presented in particle trapping results. Moreover, bigger pillars can hold more particles increasing the array trapping efficiency.

5.1 Future goals

Despite this method has been proved to be promising, more experiments has to be done to reach the final goal of CTCs separation from whole blood samples. Firstly, same experiments have to be run using a more powerful voltage amplifier, permitting to exploit high tensions at frequencies up to 200 kHz, so to cover the range of frequency (50-200 kHz) where the DEP force acting on cells changes sign and intensity. Then, tests must be made involving WBCs, RBCs and CTCs together, tuning frequency and tension to selectively trap WBCs and ensuring that side effects as Joule heating are not harmful for complete biological samples. Furthermore, design modifications should be made and tested to improve performances as throughput and flow rate and to reduce the tension applied for increased viability.

APPENDIX

APPENDIX (continued)

ROYAL SOCIETY OF CHEMISTRY LICENSE TERMS AND CONDITIONS

Apr 17, 2018

This Agreement between Mr. Enrico Grassilli ("You") and Royal Society of Chemistry ("Royal Society of Chemistry") consists of your license details and the terms and conditions provided by Royal Society of Chemistry and Copyright Clearance Center.

License Number	4331600750345
License date	Apr 17, 2018
Licensed Content Publisher	Royal Society of Chemistry
Licensed Content Publication	Lab on a Chip
Licensed Content Title	Tipping the balance of deterministic lateral displacement devices using dielectrophoresis
Licensed Content Author	Jason P. Beech,Peter Jönsson,Jonas O. Tegenfeldt
Licensed Content Date	Jun 15, 2009
Licensed Content Volume	9
Licensed Content Issue	18
Type of Use	Thesis/Dissertation
Requestor type	non-commercial (non-profit)
Portion	figures/tables/images
Number of figures/tables/images	1
Format	print and electronic
Distribution quantity	10
Will you be translating?	no
Order reference number	
Title of the thesis/dissertation	A Microfluidic device for label-free sorting of Circulating Tumor Cells
Expected completion date	May 2018
Estimated size	1
Requestor Location	Mr. Enrico Grassilli 1445 W CORTEZ ST APT 3 CHICAGO, IL 60642 United States Attn: Mr. Enrico Grassilli
Billing Type	Invoice
Billing Address	Mr. Enrico Grassilli 1445 W CORTEZ ST APT 3 CHICAGO, IL 60642 United States Attn: Mr. Enrico Grassilli
Total	**0.00 USD**

Terms and Conditions

This License Agreement is between {Requestor Name} (“You”) and The Royal Society of Chemistry (“RSC”) provided by the Copyright Clearance Center (“CCC”). The license consists of your order details, the terms and conditions provided by the Royal Society of Chemistry, and the payment terms and conditions.

RSC / TERMS AND CONDITIONS

INTRODUCTION

The publisher for this copyrighted material is The Royal Society of Chemistry. By clicking “accept” in connection with completing

APPENDIX (continued)

SPRINGER NATURE LICENSE TERMS AND CONDITIONS

Apr 16, 2018

This Agreement between Mr. Enrico Grassilli ("You") and Springer Nature ("Springer Nature") consists of your license details and the terms and conditions provided by Springer Nature and Copyright Clearance Center.

License Number	4330850101113
License date	Apr 16, 2018
Licensed Content Publisher	Springer Nature
Licensed Content Publication	Nature Protocols
Licensed Content Title	Single-cell analysis and sorting using droplet-based microfluidics
Licensed Content Author	Linas Mazutis, John Gilbert, W Lloyd Ung, David A Weitz, Andrew D Griffiths et al.
Licensed Content Date	Apr 4, 2013
Licensed Content Volume	8
Licensed Content Issue	5
Type of Use	Thesis/Dissertation
Requestor type	academic/university or research institute
Format	print and electronic
Portion	figures/tables/illustrations
Number of figures/tables/illustrations	1
High-res required	no
Will you be translating?	no
Circulation/distribution	<501
Author of this Springer Nature content	no
Title	A Microfluidic device for label-free sorting of Circulating Tumor Cells
Instructor name	Prof. Jie Xu
Institution name	University of Illinois at Chicago
Expected presentation date	May 2018
Portions	Figure 4: Principle of experimental design.
Requestor Location	Mr. Enrico Grassilli 1445 W CORTEZ ST APT 3 CHICAGO, IL 60642 United States Attn: Mr. Enrico Grassilli
Billing Type	Invoice
Billing Address	Mr. Enrico Grassilli 1445 W CORTEZ ST APT 3 CHICAGO, IL 60642 United States Attn: Mr. Enrico Grassilli
Total	0.00 USD

APPENDIX (continued)

ROYAL SOCIETY OF CHEMISTRY LICENSE TERMS AND CONDITIONS

Apr 16, 2018

This Agreement between Mr. Enrico Grassilli ("You") and Royal Society of Chemistry ("Royal Society of Chemistry") consists of your license details and the terms and conditions provided by Royal Society of Chemistry and Copyright Clearance Center.

License Number	4330860397511
License date	Apr 16, 2018
Licensed Content Publisher	Royal Society of Chemistry
Licensed Content Publication	Lab on a Chip
Licensed Content Title	Microfluidic cell sorting: a review of the advances in the separation of cells from debulking to rare cell isolation
Licensed Content Author	C. Wyatt Shields IV,Catherine D. Reyes,Gabriel P. López
Licensed Content Date	Jan 6, 2015
Licensed Content Volume	15
Licensed Content Issue	5
Type of Use	Thesis/Dissertation
Requestor type	non-commercial (non-profit)
Portion	figures/tables/images
Number of figures/tables/images	2
Format	print and electronic
Distribution quantity	10
Will you be translating?	no
Order reference number	
Title of the thesis/dissertation	A Microfluidic device for label-free sorting of Circulating Tumor Cells
Expected completion date	May 2018
Estimated size	1
Requestor Location	Mr. Enrico Grassilli 1445 W CORTEZ ST APT 3 CHICAGO, IL 60642 United States Attn: Mr. Enrico Grassilli
Billing Type	Invoice
Billing Address	Mr. Enrico Grassilli 1445 W CORTEZ ST APT 3 CHICAGO, IL 60642 United States Attn: Mr. Enrico Grassilli
Total	0.00 USD

Terms and Conditions

This License Agreement is between {Requestor Name} ("You") and The Royal Society of Chemistry ("RSC") provided by the Copyright Clearance Center ("CCC"). The license consists of

CITED LITERATURE

1. Mazutis, L., Gilbert, J., Ung, W. L., Weitz, D. A., Griffiths, A. D., and Heyman, J. A.: Single-cell analysis and sorting using droplet-based microfluidics. Nature Protocols, 8:870, 2013.

2. Wyatt Shields IV, C., Reyes, C. D., and Lopez, G. P.: Microfluidic cell sorting: a review of the advances in the separation of cells from debulking to rare cell isolation. Lab Chip, 15:1230–1249, 2015.

3. Beech, J. P., Jonsson, P., and Tegenfeldt, J. O.: Tipping the balance of deterministic lateral displacement devices using dielectrophoresis. Lab Chip, 9:2698–2706, 2009.

4. Whitesides, G. M.: The origins and the future of microfluidics. Nature, 442:368, 07 2006.

5. Manz, A., Harrison, D., Verpoorte, E., Fettinger, J., Paulus, A., Ludi, H., and Widmer, H.: Planar chips technology for miniaturization and integration of separation techniques into monitoring systems. capillary electrophoresis on a chip. Journal of Chromatography A, 593:253–258, 11 1992.

6. Toner, M. and Irimia, D.: Blood-on-a-chip. Annual Review of Biomedical Engineering, 7(1):77–103, 2005.

7. Alshareef, M., Metrakos, N., Juarez Perez, E., Azer, F., Yang, F., Yang, X., and Wang, G.: Separation of tumor cells with dielectrophoresis-based microfluidic chip. Biomicrofluidics, 7(1):011803, 2013.

8. Vaziri, A. and Gopinath, A.: Cell and biomolecular mechanics in silico. 7:15–23, 02 2008.

9. Siegel, R. L., Miller, K. D., and Jemal, A.: Cancer statistics, 2017. CA: A Cancer Journal for Clinicians, 67(1):7–30.

10. Mehlen, P. and Puisieux, A.: Metastasis: a question of life or death. Nature Reviews Cancer, 2006.

11. Howlader, N., Noone, A., Krapcho, M., Neyman, N., Aminou, R., Waldron, W., Altekruse, S., Kosary, C., Ruhl, J., Tatalovich, Z., Cho, H., Mariotto, A., Eisner, M., Lewis,

CITED LITERATURE (continued)

D., Chen, H., Feuer, E., Cronin, K., and Edwards, B.: Seer cancer statistics review. 2011.

12. Jiang, W. G., Martin, T. A., and Mansel, R. E.: Molecular detection of micro-metastasis in breast cancer. Critical Reviews in Oncology / Hematology, 43:13–31.

13. Lucci, A., Hall, C., S Lodhi, A., K Bhattacharyya, A., Anderson, A., E Xiao, L., Bedrosian, I., Kuerer, H., and M Krishnamurthy, S.: Circulating tumour cells in non-metastatic breast cancer: a prospective study. The Lancet Oncology, 13(7):688–695.

14. Zieglschmid, V., Hollmann, C., and Bcher, O.: Detection of disseminated tumor cells in peripheral blood. Critical Reviews in Clinical Laboratory Sciences, 42(2):155–196, 2005.

15. Gradilone, A., Gazzaniga, P., Silvestri, I., Gandini, O., Trasatti, L., Lauro, S., Frati, L., and Agliano, A.: . Oncol. Rep., 10:217 222, 2003.

16. Hou, J.-M., Krebs, M. G., Lancashire, L., Sloane, R., Backen, A., Swain, R. K., Priest, L. J., Greystoke, A., Zhou, C., Morris, K., Ward, T., Blackhall, F. H., and Dive, C.: Clinical significance and molecular characteristics of circulating tumor cells and circulating tumor microemboli in patients with small-cell lung cancer. Journal of Clinical Oncology, 30(5):525–532, 2012.

17. Bidard, F.-C., Fehm, T., Ignatiadis, M., Smerage, J. B., Alix-Panabières, C., Janni, W., Messina, C., Paoletti, C., Müller, V., Hayes, D. F., Piccart, M., and Pierga, J.-Y.: Clinical application of circulating tumor cells in breast cancer: overview of the current interventional trials. Cancer and Metastasis Reviews, 32(1):179–188, Jun 2013.

18. Farace, F., Massard, C., Vimond, N., Drusch, F., Jacques, N., Billiot, F., Laplanche, A., Chauchereau, A., Lacroix, L., Planchard, D., Le Moulec, S., Andr, F., Fizazi, K., Soria, J. C., and Vielh, P.: A direct comparison of cellsearch and iset for circulating tumour-cell detection in patients with metastatic carcinomas. British Journal Of Cancer, 105(1):847, 2011.

19. Hyun, K.-A. and Jung, H.-I.: Advances and critical concerns with the microfluidic enrichments of circulating tumor cells. Lab Chip, 14:45–56, 2014.

20. Miltenyi, S., Mlle, W., Weichel, W., and Radbruch, A.: High gradient magnetic cell separation with macs. Cytometry, 11(2):231–238.

CITED LITERATURE (continued)

21. Bonner, W. A., Hulett, H. R., Sweet, R. G., and Herzenberg, L. A.: Fluorescence activated cell sorting. Review of Scientific Instruments, 43(3):404–409, 1972.

22. Voldman, J.: Electrical forces for microscale cell manipulation. Annual Review of Biomedical Engineering, 8(1):425–454, 2006.

23. Gonzalez, C. F. and Remcho, V. T.: Harnessing dielectric forces for separations of cells, fine particles and macromolecules. Journal of chromatography. A, 1079(1-2):5968, June 2005.

24. Hu, X., Bessette, P. H., Qian, J., Meinhart, C. D., Daugherty, P. S., and Soh, H. T.: Marker-specific sorting of rare cells using dielectrophoresis. 102(44):15757–15761, 2005.

25. Mance, S., Chami, B., Boyer, L., Blatch, C., and Bancaud, A.: Matrix-free deterministic lateral displacement for dna separation using electro-hydrodynamic actuation in viscoelastic liquids.

26. Takahashi, K., Hattori, A., Suzuki, I., Ichiki, T., and Yasuda, K.: Non-destructive on-chip cell sorting system with real-time microscopic image processing. Journal of Nanobiotechnology, 2(1):5, Jun 2004.

27. Guo, F., Ji, X.-H., Liu, K., He, R.-X., Zhao, L.-B., Guo, Z.-X., Liu, W., Guo, S.-S., and Zhao, X.-Z.: Droplet electric separator microfluidic device for cell sorting. Applied Physics Letters, 96(19):193701, 2010.

28. Huang, Y., Joo, S., Duhon, M., Heller, M., Wallace, B., and Xu, X.: Dielectrophoretic cell separation and gene expression profiling on microelectronic chip arrays. Analytical Chemistry, 74(14):3362–3371, 2002.

29. Cummings, E. B. and Singh, A. K.: Dielectrophoresis in microchips containing arrays of insulating posts: theoretical and experimental results. Analytical Chemistry, 75(18):4724–4731, 2003.

30. Velev, O. D. and Bhatt, K. H.: On-chip micromanipulation and assembly of colloidal particles by electric fields. Soft Matter, 2:738–750, 2006.

31. Erlandsson, P. G. and Robinson, N. D.: Electrolysisreducing electrodes for electrokinetic devices. ELECTROPHORESIS, 32(67):784–790.

CITED LITERATURE (continued)

32. Tsutsui, H. and Ho, C.: Cell separation by non-inertial force fields in microfluidic systems. Mechanics Research Communications, 36(1):92 – 103, 2009.

33. Beech, J. P., Holm, S. H., Adolfsson, K., and Tegenfeldt, J. O.: Sorting cells by size, shape and deformability. Lab Chip, 12:1048–1051, 2012.

34. Huang, R., Barber, T. A., Schmidt, M. A., Tompkins, R. G., Toner, M., Bianchi, D. W., Kapur, R., and Flejter, W. L.: A microfluidics approach for the isolation of nucleated red blood cells (nrbcs) from the peripheral blood of pregnant women. Prenatal Diagnosis, 28(10):892–899.

35. Bao, D.: Deterministic sorting by electrical properties and morphology, 2017.

36. Bhattacharya, S., T Chao, z., and Ros, A.: Insulatorbased dielectrophoretic single particle and single cancer cell trapping. ELECTROPHORESIS, 32(18):2550–2558.

37. McGrath, J., Jimenez, M., and Bridle, H.: Deterministic lateral displacement for particle separation: a review. Lab Chip, 14:4139–4158, 2014.

38. Davis, J.: Micro fluidic separation of blood components through deterministic lateral displacement. Doctoral dissertation.

39. Cheng, C., Parker, D., and Taylor, C.: Quantification of Wall Shear Stress in Large Blood Vessels Using Lagrangian Interpolation Functions with Cine Phase-Contrast Magnetic Resonance Imaging, volume 30. 10 2002.

40. Inglis, D. W., Davis, J. A., Austin, R. H., and Sturm, J. C.: Critical particle size for fractionation by deterministic lateral displacement. Lab Chip, 6:655–658, 2006.

41. Beech, J.: Microfluidics Separation and Analysis of Biological Particles. Doctoral dissertation, Lund University, 2011.

42. Pohl, H., Pollock, K., and Crane, J.: Dielectrophoretic force: a comparison of theory and experiments. J Biol Phys, 6, 1978.

43. Han, S.-I., Joo, Y.-D., and Han, K.-H.: An electrorotation technique for measuring the dielectric properties of cells with simultaneous use of negative quadrupolar dielectrophoresis and electrorotation. Analyst, 138:1529–1537, 2013.

CITED LITERATURE (continued)

44. Morgan, H. and Green, N.: Ac electrokinetics: colloids and nanoparticles. Technical Report 2, 2003.

45. Han, S.-I., Joo, Y.-D., and Han, K.-H.: An electrorotation technique for measuring the dielectric properties of cells with simultaneous use of negative quadrupolar dielectrophoresis and electrorotation. Analyst, 138:1529–1537, 2013.

46. Shafiee, H., Caldwell, J. L., Sano, M. B., and Davalos, R. V.: Contactless dielectrophoresis: a new technique for cell manipulation. Biomedical Microdevices, 11(5):997, May 2009.

47. Sano, M., Caldwell, J., and Davalos, R.: Modeling and development of a low frequency contactless dielectrophoresis (cdep) platform to sort cancer cells from dilute whole blood samples. Biosensors and Bioelectronics, 30(1):13 – 20, 2011.

48. a549: general information. http://www.a549.com/, [Online accessed: 4/22/2018].

49. Hirsch, C.: Culturing a549 cells. 2014. Ver 1.0.

50. Reyes, D., Iossifidis, D., Auroux, P., and Manz, A.: Micro total analysis systems. 1. introduction, theory, and technology. Analytical Chemistry, 74:2623–2636, 07 2002.

51. Braun, S., Pantel, K., Braun, S., and Pantelb, A. K.: Clinical significance of occult metastatic cells in bone marrow of breast cancer patients. oncologist 2001; 6.

52. Seed, B.: Silanizing glassware. Current Protocols in Cell Biology, 8(1):A.3E.1–A.3E.2.